Master of Science Thesis in Electrical Engineering
Department of Electrical Engineering, Linköping University, 2016

Enhancements in LTE OTDOA Positioning for Multipath Environments

Ivar Olofsson

Master of Science Thesis in Electrical Engineering

Enhancements in LTE OTDOA Positioning for Multipath Environments

Ivar Olofsson

LiTH-ISY-EX--16/4950--SE

Supervisor: **Vladimir Savic**
ISY, Linköping University
Henrik Rydén
Ericsson Research, Ericsson AB
Sara Modarres Razavi
Ericsson Research, Ericsson AB

Examiner: **Danyo Danev**
ISY, Linköping University

Communication Systems
Department of Electrical Engineering
Linköping University
SE-581 83 Linköping, Sweden

Abstract

By using existing radio network infrastructure, a user can be positioned even where GPS and other positioning technologies lack coverage. The *LTE Positioning Protocol* (LPP) supports user *Reference Signal Time Difference* (RSTD) reports based on the *Time of Arrival* (TOA) for a *Positioning Reference Signal* (PRS). In the current reporting format, only one RSTD for each base station is considered, but for indoor environments this is easily biased due to fading and multipath issues, resulting in a *Non-Line of Sight* (NLOS) bias. With a rich *User Equipment* (UE) feedback that can represent the multipath channel for each *Base Station* (BS), the positioning accuracy can be increased. This thesis develops and evaluates a UE reporting format representing multiple TDOA candidates, and a probabilistic positioning algorithm, in terms of positioning accuracy and amount of data reported. By modeling time measurements as *Gaussian Mixture* (GM), the time information can be compressed with arbitrary resolution and used in a *Maximum-Likelihood* (ML) estimation to find the position. Results were obtained through simulation in a radio network simulator and post-processing of simulation data in Matlab. The results suggest that several TOA candidates improve the positioning accuracy, but that the largest improvement comes from a noise based threshold by increasing LOS detectability reducing the NLOS bias, while suppressing noise. The results also suggest that the accuracy for the method can be further improved by combining multiple time measurement occasions.

Acknowledgements

I would like to express my gratitude to my supervisors at Ericsson Research in Linköping, Henrik Rydén and Sara Modarres Razavi, for their insightful comments and feedback and their many readings of my drafts. With their help, I was able to stay on the right track during most of the thesis work.

I also want to thank my supervisor at Linköping University, Vladimir Savic, for his valuable comments and feedback on my report drafts, and my examiner Danyo Danev for his support during this thesis period.

Piteå, July 2016
Ivar Olofsson

Contents

List of Figures

List of Tables

Notation

Abbrevations

Notation	Meaning
3GPP	3rd Generation Partnership Project
A-GNSS	Assisted Global Navigation Satellite Systems
AOA	Angle of Arrival
AWGN	Additive White Gaussian Noise
BS	Base Station
BW	Bandwidth
CDF	Cumulative Density Function
CID	Cell ID
CIR	Channel Impulse Response
DL	Downlink
E-CID	Enhanced Cell ID
EM	Expectation Maximization
FFT	Fast Fourier Transform
GDOP	Geometrical Dilution of Precision
GM	Gaussian Mixture
GMF	GM Filter
GPS	Global Positioning System
IFFT	Inverse FFT
ISD	Inter-Site Distance
LBS	Location-Based Services
LOS	Line of Sight
LPP	LTE Positioning Protocol
LS	Location Server
LTE	Long Term Evolution
MIMO	Multiple-Input-Multiple-Output
ML	Maximum-Likelihood
NLOS	Non-Line of Sight
OFDM	Orthogonal Frequency Division Multiplexing
OLS	Ordinary Least Square
OTDOA	Observed Time Difference of Arrival

Abbrevations

Notation	Meaning
PAPR	Peak-to-Average-Power Ratio
PDF	Probability Density Function
PDP	Power Delay Profile
PMEPR	Peak-to-Mean-Envelope-Power Ratio
PRS	Positioning Reference Signal
QPSK	Quadrature Phase-Shift Keying
RAN	Radio Access Network
RB	Resource Block
RE	Resource Element
RSS	Received Signal Strength
RSTD	Reference Signal Time Difference
RTT	Round Trip Time
RX	Receiver
SINR	Signal-to-Interference-plus–Noise Ratio
SNR	Signal-to-Noise Ratio
TDOA	Time Difference of Arrival
TOA	Time of Arrival
TX	Transmitter
UE	User Equipment

Mathematical notation

Notation	Meaning
τ	time delay of path
$h[t]$	CIR
$x[t]$	PRS (with cyclic prefix)
$n[t]$	receiver noise
$y[t]$	received signal
f_s	sample frequency
N_w	search window length for PRS
$R[\tau]$	cross-correlation between PRS and $y[t]$
$R_{\text{CIR}}[\tau]$	cross-correlation between PRS and CIR
$R_n[\tau]$	cross-correlation between PRS and $n[t]$
$\tau_{\max}$	time delay of PDP maximum
$a_{\max}$	amplitude of PDP maximum
$R_{\text{norm}}[\tau]$	normalized PDP
ν	distance from origin to Rice distribution center
σ	Rice scale parameter (complex component variance)
a	peak amplitude
$a_{\text{lobe},p}(\delta)$	side lobe amplitude
$a_{\text{lobe,max}}$	maximum side lobe amplitude
$F(x;\nu,\sigma)$	Rice distribution CDF
$\hat{\sigma}_n$	PDP noise variance
β	σ scale factor for $\hat{\sigma}_n$
ζ	Rice distribution truncation amount
$p_n(a)$	probability of noise peak amplitude larger than a
$a_{\min}$	peak detection threshold
$p_{\min}$	probability of detection of noise peak
$p_{n,\max}$	probability of not disregarding noisy PDP
$\sigma_{n,\max}$	threshold variance for disregarding PDP
$\mathcal{S}_s$	CIR peak search window for TOA candidates
$N_{w,\text{LOS}}$	number of samples before $\tau_{\max}$ for $\mathcal{S}_s$
$\mathcal{S}_n$	noise window for calculating noise variance $\hat{\sigma}_n^2$
N_τ	number of time delays calculated for the PDP
$N_{n,pre}$	number of disregarded samples before $\tau_{\max}$ for $\mathcal{S}_n$
$N_{n,post}$	number of disregarded samples after $\tau_{\max}$ for $\mathcal{S}_n$
$\mathcal{P}$	set of detected peaks
$\hat{\alpha}_d$	candidate probability factor for distance penalty
α_σ	coefficient for GM variance noise dependency
$N_{\max}$	maximum number of BSs considered in position estimation

1

Introduction

The demand for mobile positioning services is increasing, mainly driven by emergency services and commercial applications [1]. With a mobile User Equipment (UE) being carried around most of the time, users connected to a *Radio Access Network* (RAN) can use *Location-Based Services* (LBS). Examples of LBS include listing of nearby restaurants, and allowing emergency services to find a caller in distress.

LTE Release 9 introduced support to the positioning methods *Assisted Global Navigation Satellite Systems* (A-GNSS), *Enhanced Cell ID* (E-CID), and *Observed Time Difference of Arrival* (OTDOA) [1]. These methods have different position accuracy and requirements, and a single method is not the best choice for every scenario. A-GNSS gives proper position accuracy but require good reception from satellites, which might not be the case in dense urban areas or indoor environments where severe shadowing can be expected. CID is a coarse technique which in its most basic form returns the position of the serving cell in the network. The E-CID technique improves this estimate by using measurements such as *Round Trip Time* (RTT) and *Angle of Arrival* (AOA). If many BSs are in range, OTDOA can give a position from combined Reference Signal Time Difference (RSTD) measurements.

The RSTD is composed by the difference in the estimated Time of Arrival (TOA) for a Positioning Reference Signal (PRS). The RSTD is the PRS TOA difference between each BS and a reference BS. A conventional method to estimate the TOA is to find the time delay at which the correlation between the PRS and the received signal has its maximum. The reason for using RSTD and not the TOA directly is that UEs generally cannot be assumed to be time synchronized with BSs. By using RSTD, the UE synchronization bias is eliminated from the measurements. Another method to remove synchronization bias is to use the RTT measurement.

The RSTD is roughly proportionate to the difference in distance to a BS and the

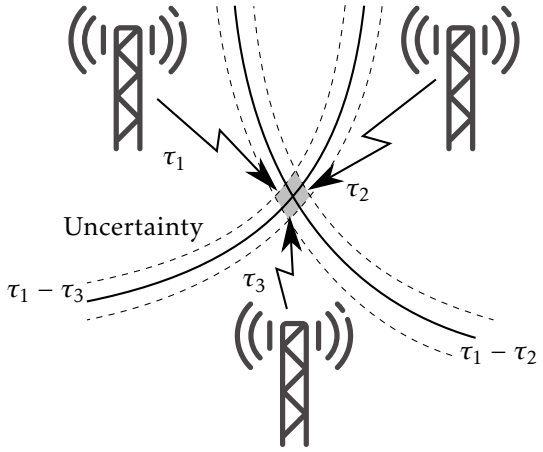

Figure 1.1: *Positioning a UE using RSTD measurements.*

reference BS from the UE. In turn, each RSTD corresponds to a parabola on which the UE position is expected. If at least two RSTD measurements are available, the UE position can be estimated for a 2D scenario. Due to uncertainty in the time measurements, the estimation has a corresponding uncertainty region. Figure 1.1 illustrates the position estimation.

1.1 Challenges in Indoor Positioning

While several technologies are applicable for positioning outdoor UEs in a RAN, alternatives for indoor UEs are limited. In indoor and dense urban areas, the radio channel suffers from shadowing and multipath issues [21]. Because of this, A-GNSS with weak satellite signals and methods based on measurements such as AOA and *Received Signal Strength* (RSS) are often unreliable . Therefore, OTDOA is usually the preferred method in these cases.

The OTDOA positioning method usually assume Gaussian distributed TOA measurement errors, which is unfeasible for indoors UEs or in other environments where the channel have shadowing and multipath properties [10, 7]. If the *Line of Sight* (LOS) is not the strongest multipath component, a delayed Non-Line of Sight (NLOS) component might be selected to estimate the TOA. This error results in TOA measurements with positive bias, and is usually the case for indoor TOA measurements. In Figure 1.2 on the next page, a channel with a strong delayed multipath component is illustrated, which could yield a positive bias.

The bias can be reduced by detecting the first multipath component instead of the strongest component. Detecting the first component over a certain power threshold reduces the bias from wrongfully selecting a late multipath component [23, 11], but there is still bias if the LOS component is undetected.

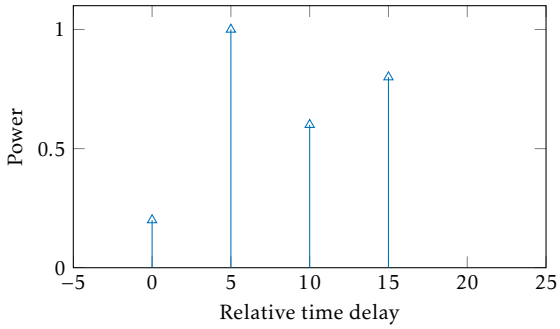

Figure 1.2: *Example CIR for multipath channel, with time delay relative to the LOS path. If the LOS path is obstructed, the LOS component will be weak and a delayed CIR component will instead be detected. This selection error results in a positive bias in the TOA estimate.*

1.2 Problem Formulation

For indoor users, the TOA error is dominated by NLOS bias, which severely decreases the position accuracy. The current specification of LTE only supports one out of several possible RSTD choices, but this estimate easily becomes biased due to indoor CIR being dominated by NLOS components. To reduce the bias, the LOS detectability can be increased. This can be achieved by allowing several uncertain time estimates, by modeling several uncertain TOA measurements with a Gaussian Mixture (GM) [10, 7]. If an estimated multipath CIR is modeled as a GM, then each GM component can be interpreted as a separate TOA candidate. A similar approach using GM to represent TDOA candidates was studied for acoustic tracking in [20], under the assumption that the LOS component is always present.

There is a need for development and evaluation of models for combining additional RSTD information, but also controlling the computational complexity. A possible improvement that is studied in this work is a reporting format featuring a GM model for the RSTD estimates, to better reflect the multipath properties [10]. This approach allows several concurrent RSTD candidates for increased accuracy, while increasing the computational complexity at the location server which estimates the position. The positioning method for multiple RSTD candidates is illustrated in Figure 1.3 on the following page. Based on this, a few questions can be formulated as follows:

- How much does the positioning accuracy increase with several RSTD candidates?
- How much additional data need to be reported by the UE?
- How much does the computational complexity increase at the UE and location server?

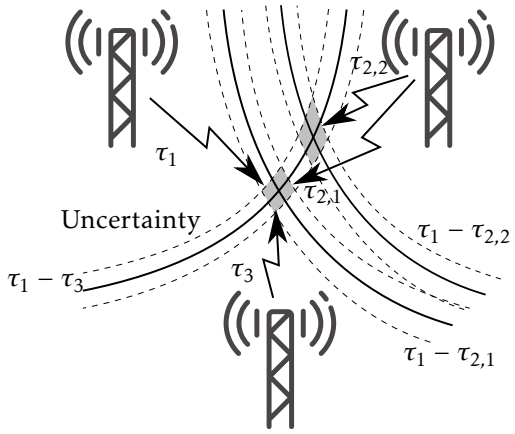

Figure 1.3: *Positioning a UE using multiple RSTD measurements per BS.*

1.3 Restrictions

This study only considers the scenario of indoor UEs and outdoor BSs agreed upon in 3GPP (*3rd Generation Partnership Project*), as this is a common scenario where position accuracy suffers from multipath channel properties and shadowing. As no channel properties specific to an indoor scenario is assumed by the method, it can also be applied to other scenarios. Further, the positioning is done in 2D to decrease the search space and also due to the low vertical accuracy which can be expected from OTDOA as seen in [23] among others.

1.4 Ethical Considerations

Until recently, the positioning capabilities standardized in 3GPP were mainly motivated and based on positioning the UE in emergency conditions [1]. While the topic is increasingly getting attention due to some other Location-Based Services (LBS), the user's security and privacy issues have always been regarded in all the enhancements considered for the network. To protect the user's privacy, most UEs require consent from the user before sending positioning information to the service provider.

1.5 Outline

The report is structured as follows: In Chapter 2, an overview of research in methods applicable to LTE indoor positioning is presented. Chapter 3 presents the OTDOA positioning method for multiple RSTD candidates. Chapter 4 gives a theoretical overview of the properties of the *Power Delay Profile* (PDP) measurement used for time delay estimation. Chapter 5 describes the method for detecting TOA candidates. In Chapter 6, the scenario and simulation setup are

presented. Chapter 7 presents the results for the timing and positioning methods. Chapter 8 evaluates and discuss the results and method, and also concludes the study questions, and suggest topics for further study.

2

Background on Indoor Positioning

This chapter presents an overview of previous research in OTDOA positioning and some related methods that can be applicable for indoor positioning in LTE. The focus is on multipath environment scenarios, such as indoor UEs and outdoor BSs. The methods covered in this chapter are pattern recognition, also known as fingerprinting, TOA and OTDOA methods with NLOS bias compensation, and finally hybrid TOA and AOA methods.

2.1 Fingerprinting

An emerging positioning method is fingerprinting, where stored radio channel metrics for each position are matched against UE measurements to yield a position estimate. Fingerprinting methods can provide increased accuracy over triangulation and multilateration methods in NLOS conditions [21], as it is the pattern features of the metrics for each location that is used, and no assumption of LOS is required. The obvious drawback is that the pattern features of each location have to be measured prior to position estimation, and that locations with similar pattern features might be hard to distinguish. Also, in dynamic environments, a previously collected pattern might not remain accurate. For emergency positioning, the assumption that most locations already have stored measurements might not be viable.

2.2 Time of Arrival Positioning

For indoor positioning, TOA and OTDOA have often been used due to their robustness [21]. The two methods are closely related, where OTDOA is chosen if the UE cannot be assumed to be time synchronized with the BSs.

An essential part of TDOA positioning methods is the estimation of TOA. A conventional method to estimate propagation time delay is by calculating the cross-correlation of the received signal y with the transmitted signal x [11], in this case the PRS. A simple TOA estimate is the instance where the absolute value of the cross-correlation $R[\tau]$, the Power Delay Profile (PDP), has its maximum peak [16, 20]. This estimate is the best if the LOS component is the strongest. The TOA estimate τ is then given by

$$\tau = \arg\max_{\tau} |R[\tau]| = \arg\max_{\tau} \left| \sum_{i=0}^{N_w-1} x^*[i-\tau]y[i] \right| \tag{2.1}$$

where $(\cdot)^*$ denotes the complex conjugate, and N_w is the length of the search window.

If the multipath channel experiences severe shadowing in the LOS path, a delayed path might instead have the strongest peak in the PDP. A case where this would be the case is illustrated in Figure 1.2 on page 3. To compensate for this, an earlier PDP peak can instead be selected by using a threshold. This is a generalization of the maximum peak detection, which instead can be seen as first-peak detection. This approach is studied in [23] for OTDOA positioning, and in [11] for OTDOA timing accuracy. These studies indicate that first-peak detection can significantly improve OTDOA timing and positioning accuracy for indoor and urban environments, if the threshold is chosen appropriately.

2.2.1 Non-Line-of-Sight Bias Compensation

Several methods have been proposed to further reduce the positioning error stemming from NLOS TOA measurements. This is useful as many UE assisted positioning methods use measurements from the UE, but the position calculation is done at a location server. As the UE do not know the estimated position during the TOA measurements, any iterative NLOS compensation of TOA measurements depending on the position estimation have to be done at the location server.

The positioning error from NLOS bias in TOA measurements can be reduced by detecting and omitting NLOS measurements, by weighting measurements based on TOA residuals, or by correcting the bias if the NLOS error distribution can be estimated. The TOA residual is defined as the difference between the estimated and measured TOA for a BS, where the estimated TOA is given by the estimated position. The residual is essentially a measure of how well each TOA measurement fits the estimated position. Therefore, the idea of these methods is to identify ill-fitting TOA measurements by their residuals and reduce their impact in the position estimation.

The theory for TOA positioning methods is also valid for TDOA, if LOS measurement is assumed for the reference BS. This assumption translates any NLOS bias in TOA measurements directly to NLOS bias in TDOA measurements. However, for indoor and urban UEs, an LOS BS might be neither present nor identifiable.

2.2.2 Residual Weighting

A residual weighting algorithm for TOA positioning was proposed in [2]. Using a positioning method where the TOA residual of all measurements are minimized, a position is calculated for each possible subset of at least three BSs. The final position is the weighted average of the subset positions, with the inverse of the residuals of the sets as a weighting factor. The subsets including NLOS measurements receive a small weight due to large bias error, and sets with a majority of LOS measurements receive a larger weight. Essentially, this method aims to include NLOS bias information to reduce impact from NLOS measurements.

This approach is feasible when few measurements are available and only a few suffer from NLOS, as the subset count otherwise will get very large and an NLOS majority reduces the effectiveness of the weighting. Also, it is not always true that the reference BS is LOS, or that an LOS BS can be identified reliably. Therefore, a residual weighting algorithm do not necessarily have a positive bias for TDOA methods, which reduces the applicability of this method for indoor positioning.

2.2.3 Bias Estimation

In [4] and [3], the residual weighting algorithm in [2] is expanded with estimation of NLOS bias. Measurements with a TDOA residual over a chosen threshold are tagged as NLOS. The position is then given by a ML estimator, assuming exponential distributions with known means for the NLOS errors. In [3], the weighting step also include prior probability of receiving an NLOS measurement.

As found in [9], the residual weighting algorithm is useful when there are at least four LOS BSs available for the UE, while bias correction have insignificant impact if the NLOS bias is small. Further, [18] studied the effect of poorly located UEs outside the convex hull of BSs and found that the residual weighting algorithm underestimate the bias error under those conditions. In other words, residual weighting might improve accuracy if the NLOS biases are large and the UE is surrounded by BSs.

2.2.4 Omitting NLOS Measurements

If no prior information about the NLOS error distribution or probability is known, e.g. as a mixture model, an alternative approach is to omit detected NLOS measurements from the position calculation if allowed. Measurements suffering from NLOS conditions can often be detected by subset residuals as in [2],[4], and [3], but if measurements from more than a few BSs are used, the computational complexity can grow quickly.

Another method is based on sequential TOA measurements, where the TOA measurement variance of each BS is used to identify NLOS condition. If NLOS multipath components are assumed to have a larger variance in TOA, a variance threshold detection can be applied for a series of TOA measurements to identify NLOS components. This is studied in [22] where the variation of TOA measurements from each BS were used to omit NLOS measurements. The value of this

method is the computational simplicity which allows it to be used if an abundance of measurements are available.

2.3 Time Difference of Arrival

As presented in the previous section, the methods for positioning using TOA and OTDOA measurements are often the same. If the reference BS is LOS, the NLOS bias is positive and the same for OTDOA and TOA. However, if no LOS BS can be reliably detected, the underlying assumption of a LOS reference BS is not valid which renders residual weighting unreliable. Further, simply disregarding NLOS measurements is not a satisfactory method if most measurements are NLOS.

2.4 Hybrid TOA and AOA Methods

The previously mentioned methods for dealing with NLOS bias in TOA and TDOA measurements focus on the residual and variance properties of NLOS measurements. Other approaches to modeling a multipath channel include scattering models, where single-bounce models are used to estimate the LOS TOA from NLOS TOA and AOA measurements.

In [14] and [13], the LOS TOA is estimated by assuming the measured TOA components stem from random reflections from a geometrical scatter model, which is assumed to be known for different BSs and UE positions. For a certain scatter model, a probability distribution for mean and variance is expected. Based on the measured TOA statistics, the position of the UE can then be estimated, in ML sense or other. The drawback of this method is the requirement of a geometrical scatter model of the environment, which might not be readily available or sufficiently accurate.

In *Multiple-Input-Multiple-Output* (MIMO) systems where both transmitter and receiver have multiple antennas, estimation of AOA is possible at both UE and BS. With an AOA estimate at both ends, a hybrid positioning method using both uplink and downlink AOA and TOA measurements removes the need of a prior scattering environment model. Positioning methods using the bidirectional AOA and TOA have been proposed in [17], [24], and [19]. By using transmitter and receiver angles and time of flight for the LOS and single-bounce NLOS components, the UE position can be estimated.

One gain of using the bidirectional AOA and TOA metrics is that the method potentially only requires one BS, and that NLOS conditions are valid if paths only change direction once. The method essentially increase the utility of the AOA measurement by allowing several single-bounce paths instead of only the LOS path. However, the method relies on effective identification of single-bounce and multi-bounce paths. If single-bounce paths cannot be identified reliably, possibly due to a lack of single-bounce paths, the method would likely suffer. With this in consideration, for indoor UEs there might be too many multi-bounce signals for the method to work properly.

3

OTDOA Positioning Method

This chapter first introduces the general OTDOA positioning method, then describes the applied optimization problem which was used for positioning estimation. Later the Maximum-Likelihood (ML) variant for multiple TDOA candidates is presented, along with how the complexity grows with an increased amount of measurements.

3.1 OTDOA Positioning

The OTDOA positioning method is based on TDOA measurements observed at the UE, which are sent as RSTD reports to the location server. The UE RSTD measurements are then used to calculate a position estimate by multilateration of the UE. In this section, the base equations for estimating a position from TDOA measurements are presented.

If BS i and UE are not synchronized in their time measurements, the measured propagation time $\tilde{t}_i$ is

$$\tilde{t}_i = t_i + t_0 \tag{3.1}$$

where t_0 is the time offset between BS and UE, and t_i is the true propagation time. Assuming synchronized BSs, this unknown offset t_0 can be eliminated by forming the difference between two TOA measurements, known as the TDOA. The TDOA t_{ij} between BS i and BS j is

$$\begin{aligned} t_{ij} &= \tilde{t}_i - \tilde{t}_j = t_i + t_0 - (t_j + t_0) && (3.2)\\ &= t_i - t_j && (3.3) \end{aligned}$$

and for a UE position $\mathbf{x}$ and BS positions $\mathbf{x}_i$ and $\mathbf{x}_j$, it is

$$t_{ij} = (\|\mathbf{x} - \mathbf{x}_i\| - \|\mathbf{x} - \mathbf{x}_j\|)/c \tag{3.4}$$

$$= \left(\sqrt{(x - x_i)^2 + (y - y_i)^2} - \sqrt{(x - x_j)^2 + (y - y_j)^2}\right)/c \tag{3.5}$$

where c is the speed of light. To estimate the position, a set of TDOA measurements can be considered in an optimization problem where some residual term is minimized and the position with the minimum residual term is selected.

3.2 Positioning Reference Signal

In LTE, to allow UEs to estimate RSTD for OTDOA positioning, a specific Positioning Reference Signal (PRS) is transmitted by BSs. The PRS sequence is defined [7] by

$$r_{l,n_s}[m] = \frac{1}{\sqrt{2}}(1 - 2c[2m]) + j\frac{1}{\sqrt{2}}(1 - 2c[2m+1]), \tag{3.6}$$

where $m = 0, 1, \ldots, 2N_{\text{RB}}^{\text{max,DL}} - 1$, $N_{\text{RB}}^{\text{max,DL}}$ is the largest number of *Downlink* (DL) *Resource Block*s (RB), n_s is the slot number within a radio frame, l is the *Orthogonal Frequency Division Multiplexing* (OFDM) symbol number within the slot, and $c[\,\cdot\,]$ is a 31–length Gold sequence[1].

The PRS sequence is mapped to QPSK-modulated *Resource Element*s (RE) with six possible cell-specific frequency shifts [7]. The mapping to resource elements in a radio frame is illustrated in Figure 3.1 on the facing page. This OFDM configuration allows six different PRSs to be transmitted simultaneously without interference. Assume the PRS is mapped to resource blocks which yield a transmitted signal sequence $R_{l,n_s}[k]$ in the frequency domain as

$$R_{l,n_s}[k] = \begin{cases} r_{l,n_s}[m], & \text{if there is an } m \text{ mapped to } k, \\ 0, & \text{otherwise,} \end{cases} \tag{3.7}$$

where $k = 0, 1, \ldots, N_{\text{FFT}} - 1$, and N_{FFT} is the size of the *Fast Fourier Transform* (FFT). The transmitted signal sequence in time domain is given by the *Inverse FFT* (IFFT) as

$$x_{l,n_s}[n] = \sqrt{\frac{P}{N_{\text{FFT}}}} \sum_{k=0}^{N_{\text{FFT}}-1} R_{l,n_s}[k] \exp\left(j\frac{2\pi kn}{N_{\text{FFT}}}\right), \tag{3.8}$$

where P is the transmitted power from the BS, and $n = 0, 1, \ldots, N_{\text{FFT}} - 1$.

Consecutive PRS subframes, known as a positioning occasion, are transmitted periodically in LTE networks, where the period and number of consecutive subframes are selected in a trade-off between positioning accuracy and overhead [7]. The PRS is sent in subframes with no transmission on data channels to increase

[1] The Gold sequence is a pseudo-random sequence which is generated differently based on the *Cell ID* (CID) of the transmitting BS.

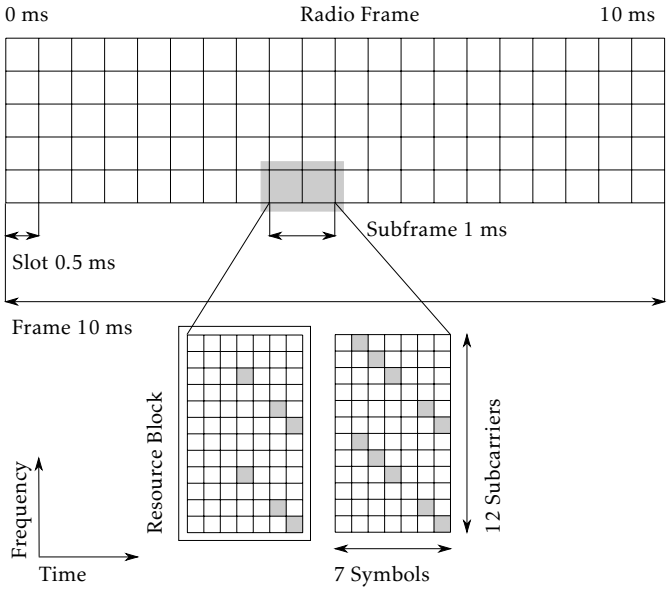

Figure 3.1: *Example PRS resource element mapping in an LTE radio frame. Allocated PRS resource elements in two resource blocks of a subframe is filled with gray.*

hearability [7]. Therefore, in perfectly synchronized networks, the PRS is only interfered by other PRSs with the same frequency shift. To minimize this interference source, the PRS from each BS can be periodically muted [7]. This muting essentially implements time–frequency multiplexing for the PRS. For example, if twelve BSs are transmitting PRSs in an area, ideally only six would transmit at a time, each with a unique frequency shift. Therefore, a muting pattern where each PRS is only sent every other positioning occasion can be applied in the area.

By using muting, the UE is able to detect weak PRS with practically no interference and only additive thermal noise [6]. In this study, an ideal muting case is considered, while a case without muting also is evaluated as a worst case scenario. However, in most practical scenarios there is network planning which aims to reduce interference, which makes the non-muted scenario less relevant.

3.3 Channel Model

To represent the outdoor-to-indoor channel, a multipath channel model is used. In a multipath channel, the CIR consists of several lagged components other than the Line of Sight (LOS) component. Due to fading and shadowing, the strongest component might not correspond to the LOS component. This easily results in a biased time estimate if only the strongest peak is considered.

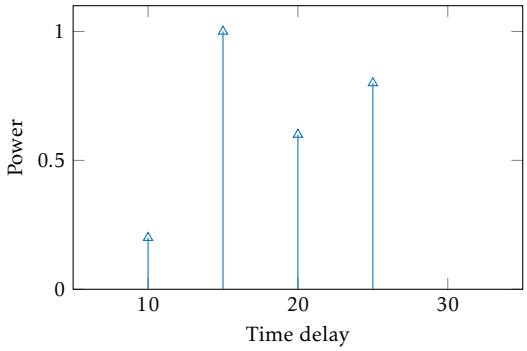

Figure 3.2: *Tapped delay line CIR for a multipath channel. If the LOS path is obstructed, the LOS component will be weak and a delayed CIR component might be detected instead. This selection error results in a positive bias in the TOA estimate.*

In this study, the multipath CIR $h[t]$ is modeled as a tapped delay line

$$h[t] = \sum_{l=1}^{L} a_l \delta[t - \tau_l] \tag{3.9}$$

where L is the path count, a_l is an amplitude coefficient, τ_l is the delay for each path, and $\delta[t]$ is the delta function

$$\delta[t] = \begin{cases} 1, & t = 0 \\ 0, & t \neq 0 \end{cases} \tag{3.10}$$

which results in the CIR consisting of impulses of amplitude a_l at sample time τ_l. An illustration of the channel model is found in Figure 3.2. As the PRS x is transmitted over the channel, we get the received signal y as

$$y[t] = h[t] * x[t] + n[t] \tag{3.11}$$

where x is given by the transmitted signal sequences in Equation (3.8) on page 12 and a cyclic prefix, $(*)$ denotes the convolution operation and n is *Additive White Gaussian Noise* (AWGN).

3.4 Gaussian Mixture for TOA Probability

As this report studies the accuracy gain from multiple TOA candidates, a method for representing several simultaneous TOA candidates for each BS is required. Conventional models with a single measurement considered usually assumes Gaussian distributed measurement error. In this work, a Gaussian Mixture (GM) is used for this purpose.

With the channel model described previously, we have several paths with varying power. Depending on power, several of the paths have the chance of being detected as the first CIR component. As the best TOA candidate is that of the first detected path, it is feasible to consider several candidates to increase the probability of including the true first path. With several candidates, it is necessary to assign a weight to each candidate. This weight is chosen as the probability of each candidate being the first detected path. The detection and probability of each TOA candidate being the first path is described later in Chapter 5 on page 31, but a set of TOA candidates with assigned weights are assumed to be available for the rest of this chapter.

Ideally, a set of TOA candidates would have a probability of one for the true LOS TOA candidate, and zero for the rest. In practice however, most approximated probabilities will be non-zero due to uncertainty of which TOA candidate is the first path. It is also possible that the LOS is too weak to be detected and therefore is missing in the set of TOA candidates. In that case, the first arriving path would be the best candidate and should preferably have the largest weight. If the first path is included as a candidate and given a non-zero weight, the positioning accuracy should be better than if only the first certain path was considered. This implies that the TOA measurement can be modeled as a Gaussian Mixture (GM) with a Gaussian component for each candidate.

Given a set of TOA candidates for each BS, the following model for RSTD measurements is proposed. Let the measured TDOA $\tilde{t}_{ij}$ for a set of $N > 2$ BSs, with the first as reference, be

$$\tilde{t}_{i1} = t_{i1} + (n_i - n_1) = (t_i + n_i) - (t_1 + n_1). \tag{3.12}$$

where $i = 2, \ldots, N$ and the noise n_i are assumed to be mutually independent and distributed as GM. The GM distribution of the noise is

$$n_i \sim \sum_{k=1}^{K_i} p_{i,k} \mathcal{N}(m_{i,k}, \sigma_{i,k}^2). \tag{3.13}$$

where K_i is the number of candidates for BS i, and the mixture parameter set $\{K_i, p_{i,k}, m_{i,k}, \sigma_{i,k}\}$ can vary among BSs and are assumed to be known due to empirical evidence. The parameter $p_{i,k}$ reflects the probability of each candidate being the first detected (or LOS) path, $m_{i,k}$ reflects the time delay relative to the true LOS path, and $\sigma_{i,k}$ describes the timing uncertainty of each candidate. The selection of these parameters are further discussed in Section 6.3 on page 40.

3.5 Position Estimation

To estimate the position, the Maximum-Likelihood (ML) method is used. For this method, the *Probability Density Function* (PDF) of the combined RSTD measure-

ments is required. This joint function[2] is

$$p(\tilde{t}_{21},...,\tilde{t}_{N1}) = \int p(\tilde{t}_{21},...,\tilde{t}_{N1}|n_1)p(n_1)dn_1 = \int \prod_{i=2}^{N} p(\tilde{t}_{i1}|n_1)\cdot p(n_1)dn_1 \quad (3.14)$$

where $p(\tilde{t}_{21},...,\tilde{t}_{N1}|n_1)$ has been split due to the noise being independent for a given n_1.[3] In turn, due to the GM distribution of the noise n_i, we have

$$p(\tilde{t}_{i1}|n_1) \sim \sum_{k_i=1}^{K_i} p_{i,k_i}\mathcal{N}(t_{i1} - n_1 + m_{i,k_i}, \sigma^2_{i,k_i}). \quad (3.15)$$

With N BSs, Equation (3.14) is a product of $N-1$ sums of GM components in an integral over n_1. Taking into consideration that a product of Gaussian functions is also Gaussian, the product of sums can be expressed as a single sum of $\prod_{i=2}^{N} K_i$ Gaussian functions. Since also the convolution of Gaussian functions is Gaussian, we get that the integral in Equation (3.14) can be expressed as a single sum of $\prod_{i=1}^{N} K_i$ Gaussian functions. Knowing this, the integral can be rewritten into closed-form after some algebraic exercise.

To simplify the function, a residual term is introduced as

$$r_{i,k_i} = \tilde{t}_i - (t_i + m_{i,k_i}). \quad (3.16)$$

The closed-form version of Equation (3.14) is

$$p(\tilde{t}_{N1},...,\tilde{t}_{21}) = \sum_{k_N}^{K_N}\cdots\sum_{k_2}^{K_2}\sum_{k_1}^{K_1} c_{k_1,k_2,...,k_N}\cdot\exp\left(\frac{\mu^2_{k_1,k_2,...,k_N} - \lambda_{k_1,k_2,...,k_N}}{2\sigma^2_{k_1,k_2,...,k_N}}\right), \quad (3.17)$$

where

$$c_{k_1,k_2,...,k_N} = (2\pi)^{-\frac{N-1}{2}}\frac{\prod_{i=1}^{N} p_{i,k_i}}{\sqrt{\sum_{i=1}^{N}\left\{\prod_{j=1,j\neq i}^{N}\sigma^2_{j,k_j}\right\}}}, \quad (3.18)$$

$$\mu_{k_1,k_2,...,k_N} = \frac{\sum_{i=1}^{N}\left\{\left(\prod_{j=1,j\neq i}^{N}\sigma^2_{j,k_j}\right)r_{i,k_i}\right\}}{\sum_{i=1}^{N}\left\{\prod_{j=1,j\neq i}^{N}\sigma^2_{j,k_j}\right\}}, \quad (3.19)$$

$$\lambda_{k_1,k_2,...,k_N} = \frac{\sum_{i=1}^{N}\left\{\left(\prod_{j=1,j\neq i}^{N}\sigma^2_{j,k_j}\right)r^2_{i,k_i}\right\}}{\sum_{i=1}^{N}\left\{\prod_{j=1,j\neq i}^{N}\sigma^2_{j,k_j}\right\}}, \quad (3.20)$$

$$\sigma^2_{k_1,k_2,...,k_N} = \frac{\prod_{i=1}^{N}\sigma^2_{i,k_i}}{\sum_{i=1}^{N}\left\{\prod_{j=1,j\neq i}^{N}\sigma^2_{j,k_j}\right\}}. \quad (3.21)$$

[2] disregards the scaling factor for total probability of one

[3] The independence of each TDOA measurement is only approximate, as all depend on the distribution of n_1. In this case, assuming independence yields a probability function that is independent of the chosen reference cell.

Given this joint function in Equation (3.17) on the facing page, the likelihood of the RSTD for the BSs can be calculated for any given true TOA. For each position, the likelihood is given by the mixture parameters and the expected TOA $\tilde{t}_i$ for the position. This expected TDOA is related to the GM TOA candidates through the residual term r_{i,k_i}.

3.6 Computational Complexity

One of the aims in the problem formulation was to determine the computational complexity of the method. The expression for the PDF is a sum of exponentials, which is an unfortunate form to optimize on in terms of computational complexity. Merging of clustered Gaussian functions to reduce complexity is possible. Another simplifying approximation is purging of components with insignificant contribution, which depends on the chosen distribution of mixture parameters. Also, assuming a common variance $\sigma_{i,k} = \sigma$ can help to simplify the expression.

The computational complexity of Equation (3.17) on the preceding page is $\mathcal{O}(N \prod_{i=1}^{N} K_i)$. Assuming a common amount of mixture components $K_i = K$ yields the complexity $\mathcal{O}(NK^N)$; for $N = 5, K = 4$ approximately 5,120 operations are required, but for $N = 10, K = 4$ a staggering 10,485,760 operations are required. This can be compared to the case with only single candidates $K_i = 1$, in which case the complexity is simply $\mathcal{O}(N)$. This stresses the need to either restrict the number of measurements, or further simplify Equation (3.17) on the facing page.

4

Power Delay Profile Properties

In this chapter, the properties of the Power Delay Profile (PDP) measurement are presented. The auto-correlation of the PRS is linked to detectability of LOS TOA in the PDP, and also how the PDP is influenced by noise. Based on the PDP properties, a peak detection threshold for TOA candidates and a hearability threshold for PDP measurements are derived. Finally, PDP windows for threshold selection and TOA detection are presented.

4.1 Power Delay Profile Convolution

The proposed TOA estimation is based on PDP, so to understand the proposed method, the fundamental properties of this measurement should be studied. The PDP is the absolute value of the correlation between the transmitted PRS and the received signal. Therefore, properties of the PRS correlation can be transferred to the PDP. The PRS correlation $R[\tau]$ consists of the CIR h correlation and noise n correlation. The PRS correlation at time delay τ is

$$R[\tau] = \sum_{i=0}^{N_w-1} x^*[i-\tau]y[i] = \sum_{i=0}^{N_w-1} x^*[i-\tau](h[i] * x[i] + n[i]) \tag{4.1}$$

where $(\cdot)^*$ denotes the complex conjugate, $(*)$ the convolution operation, and N_w is the search window length for the PRS. The correlation can be written as a sum

$$R[\tau] = R_{\text{CIR}}[\tau] + R_n[\tau] \tag{4.2}$$

where, using the associative property of convolution for an alternative form of Equation (4.1) on the previous page,

$$R_{\text{CIR}}[\tau] = \sum_{i=-\tau}^{N_w-1-\tau} (x^*[i] * x[-i])h[i+\tau] \tag{4.3}$$

$$R_n[\tau] = \sum_{i=0}^{N_w-1} x^*[i-\tau]n[i] \tag{4.4}$$

are defined for CIR h and noise n contribution respectively. Note that CIR h is convoluted with the PRS auto-correlation.

Based on Equation (4.2) on the preceding page, the following notation is introduced to ease further discussion regarding PDP.

Definition 4.1. *CIR peaks* are PDP peaks due to the CIR correlation $R_{\text{CIR}}[\tau]$.

Definition 4.2. *PDP noise* is the PRS–noise correlation $R_n[\tau]$ in Equation (4.4).

Definition 4.3. *Noise peaks* are PDP peaks stemming from PDP noise $R_n[\tau]$.

4.2 PRS Autocorrelation

As seen in the PDP calculations, the PRS autocorrelation is convoluted with the CIR. This is used to estimate the TOA of the CIR components by detecting peaks in the PDP. Therefore, to achieve good detection of LOS and other CIR components, knowledge about the PRS autocorrelation is required.

The autocorrelation for the PRS and sampling rate used in this study is illustrated in Figure 4.1 on the facing page. This autocorrelation can be fitted to a sinc function

$$\text{sinc}(x) = \begin{cases} \frac{\sin(x)}{x}, & x \neq 0, \\ 1, & x = 0, \end{cases} \tag{4.5}$$

as seen in the figure. Due to its nature, there will be side lobes beside the main CIR peaks for high SNR. For high SNR values, these side lobes can be considered the main source of potential detection errors. For lower SNR values, these can be assumed to be almost insignificant and noise is seen as the main error contributor. Therefore, the detection threshold should be based on both noise level and contribution of side lobes from nearby peaks to achieve a robust noise suppression for all SNR values. An illustration of PDPs for low and high SNR are illustrated in Figure 4.2 on the next page and Figure 4.3 on page 22. In these figures, it can be seen that the strongest peak is not always the best choice, and that multiple TOA candidates can increase detection of the LOS TOA peak.

As the autocorrelation of the PRS has a distinct peak lobe apart from side lobes, CIR peaks in the PDP provide information about the CIR, and in turn, the TOA of the channel paths. As seen in Equation (4.3), the noise free PDP essentially consists of superposed PRS autocorrelations. Therefore, by considering CIR peaks from the PDP, multipath components can be detected and taken into consideration when selecting TOA candidates.

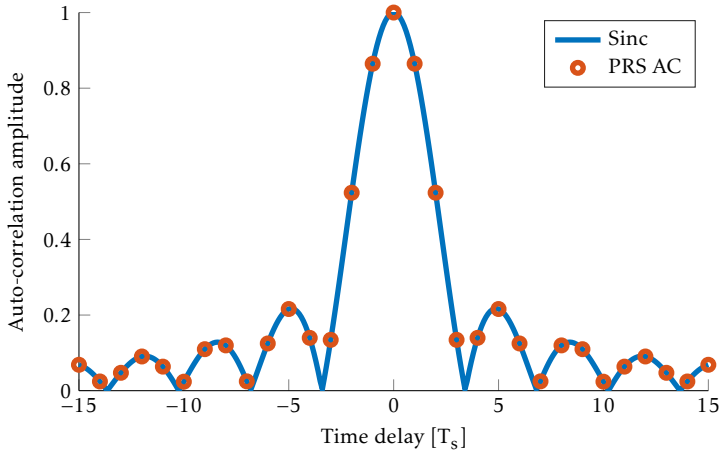

Figure 4.1: *Autocorrelation amplitude of the PRS, with lag expressed in sample periods at the horizontal axis. The* sinc*-function form can be recognized by the main lobe and side lobes amplitudes.*

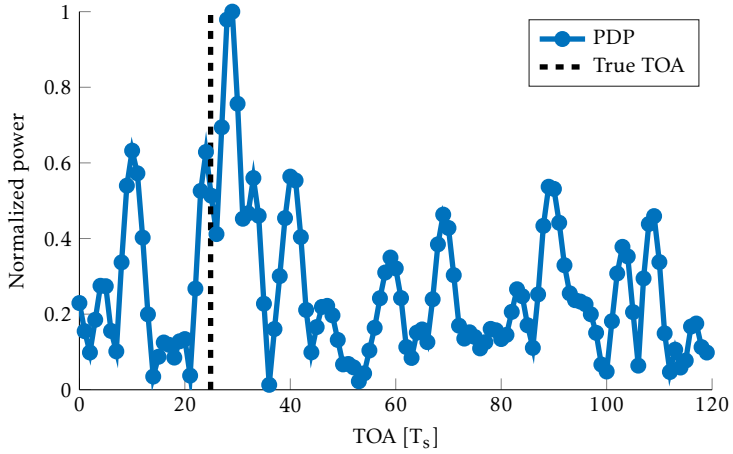

Figure 4.2: *Example PDP measurement for low SNR. A strong preceding noise peak has similar amplitude as the true TOA peak, which highlights the difficulty in distinguishing CIR peaks from noise peaks.*

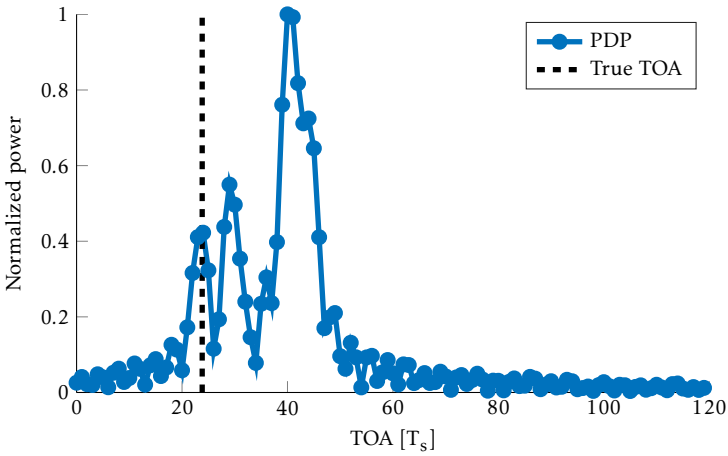

Figure 4.3: *Example PDP measurement for high SNR. For high signal strengths, the CIR peak detectability is mainly affected by side lobe suppression. It is also obvious that the strongest peak is not the best TOA estimate.*

4.3 PDP Noise Peaks

An essential feature of the detection algorithm is to yield few false detections by noise suppression. The proposed method is based on choosing a certain probability of false detections, that is detecting noise peaks. This probability can be expressed if the amplitude distribution of noise peaks is known. By using a low probability of false detections, a robust noise suppression can be achieved while detecting CIR peaks. For a higher probability, weaker CIR peaks are also detected, but the false detections increase. In this section, the distribution is derived by considering noise and PDP properties.

In this simulation study, the noise n at the receiving UE consist of two complex independent Gaussian components with equal variance σ^2 and zero mean. The noise amplitude follow a Rayleigh distribution, which can be used to express properties of the PDP noise.

4.3.1 PDP Noise

As the PDP noise is the PRS–noise correlation $R_n(t)$ in Equation (4.4) on page 20, it can be expected to have similar properties as the channel noise. Therefore, the amplitude of noise peaks is assumed to be related to the Rayleigh distribution. Further, PDP samples which are close in time will not be independent due to the convolution. Figure 4.2 on the previous page illustrates a noisy PDP where dependency among the samples clearly can be seen, with distinct peak lobes. For example, at $T_s = 10$ a strong noise peak can be seen to occur previous to the LOS TOA peak. If only a single candidate is reported, the LOS TOA peak could be

ignored and a false detection of the noise peak might be reported.

The difficulty of estimating the TOA based on the PDP is to correctly identify CIR peaks from noise peaks. For this to be a problem, the CIR and noise peaks need to have similar characteristics. Therefore, CIR and noise peaks are assumed to be practically indistinguishable apart from differences in amplitude.

4.3.2 PDP Side Lobes

Apart from noise, the side lobes of the PRS autocorrelation also influence the detectability of CIR peaks. To avoid false detections of these side lobes, their properties also have to be considered.

A simple way to model the side lobe contribution is to adjust the expected noise distribution for each detected peak based on side lobes from neighboring peaks. If the noise n variance of each complex component is σ^2 and the expected amplitude of side lobes from neighboring peaks is ν, the combined amplitude of both noise and side lobes can be described as complex Gaussian with non-zero mean ν. By using this combined measurement, the side lobes can be seen as part of the PDP noise where the side lobe amplitude is the noise mean.

The mean ν can be calculated by assuming that the side lobe contribution of all neighboring peaks are mutually orthogonal and independent of each other. This yields

$$\nu_{p_k} = \sum_{p \in \mathcal{P},\ p \neq p_k} a^2_{\text{lobe},p}(|\tau_p - \tau_{p_k}|) \tag{4.6}$$

where p_k is the peak under consideration, $\mathcal{P}$ is the set of neighboring peaks, $a_{\text{lobe},p}$ is the amplitude of side lobes for peak p, and $|\tau_p - \tau_{p_k}|$ is the time separation between peaks. The detection of $\mathcal{P}$ is described in the following chapter, and the derivation of $a_{\text{lobe},p}$ is discussed in the following subsection.

This model can be seen as an overestimated average, as the orthogonality assumption results in additional neighboring peaks always increasing the expected level, which is not the case as the side lobe peaks do not necessarily coincide, and constructive and destructive interference of complex amplitudes occur. However, in case of coinciding and constructively interfering side lobes, the amplitude might be underestimated, but this case is assumed to be an outlier relative to other cases and is therefore disregarded in the approximation. Therefore, in case the expected complex amplitude of the side lobes is known, a more exact estimated average could be possible by also considering side lobe interference. This is a possible improvement of the model for future studies.

4.3.3 Side Lobe Amplitude

As earlier discussed and shown in Figure 4.1 on page 21, the PRS autocorrelation consists of a strong main lobe and side lobes and can be fitted to a sinc function. Therefore, the side lobe amplitude of CIR peaks can be derived from the sinc

function. As the sinc function is given by

$$\operatorname{sinc}(x) = \begin{cases} \frac{\sin(x)}{x}, & x \neq 0, \\ 1, & x = 0, \end{cases} \tag{4.7}$$

the expected amplitude of side lobes at distance x from the main lobe peak can be expressed as

$$a_{\text{lobe}}(x) = \frac{1}{x}. \tag{4.8}$$

Considering that the side lobe peaks begin at a distance from the main lobe peak, this should be reflected in the expected amplitude to avoid excessive expected amplitudes close to the main lobe. A simple way to achieve this is to cap the amplitude to that of the strongest side lobe peak. As this amplitude is $a_{\text{lobe,max}} \approx 0.22$, we get

$$a_{\text{lobe}}(x) = \min\left(\frac{1}{x}, a_{\text{lobe,max}}\right). \tag{4.9}$$

To get the side lobe amplitude of CIR peaks, we need an appropriately scaled distance x and the CIR peak amplitude a_p. Denote the width of the main lobe of the PRS autocorrelation as w, expressed in sample periods. As the width of the sinc main lobe is 2π, which is directly retrieved from the zero-crossings of sin at $\pm\pi$, we have

$$a_{\text{lobe},p}(\delta) = a_p \cdot a_{\text{lobe}}\left(\frac{2\pi}{w}\delta\right) \tag{4.10}$$

where δ is the distance to the peak, expressed in samples.

4.3.4 Amplitude Distribution of Noise Peaks

In previous subsections, the contribution from noise and side lobes to the amplitude distribution of noise peak were discussed. When also considering side lobes, the noise peak distribution were assumed to have a non-zero mean ν, based on the expected side lobe amplitude from neighboring peaks. Due to its non-zero mean, the combined side lobe and noise amplitude follow the Rice distribution, illustrated in Figure 4.4 on the next page. The *Cumulative Density Function* (CDF) is

$$F(x;\nu,\sigma) = \int_{x/\sigma}^{\infty} t \exp\left(-\frac{t^2 + \left(\frac{\nu}{\sigma}\right)^2}{2}\right) I_0\left(t\frac{\nu}{\sigma}\right) dt \tag{4.11}$$

where I_0 is the modified Bessel function

$$I_0(x) = \sum_{m=0}^{\infty} \frac{1}{m!^2}\left(\frac{x}{2}\right)^{2m}. \tag{4.12}$$

The Rice distribution approaches a Gaussian distribution with mean ν and variance σ^2 when the ratio ν/σ is large, and approaches a Rayleigh distribution

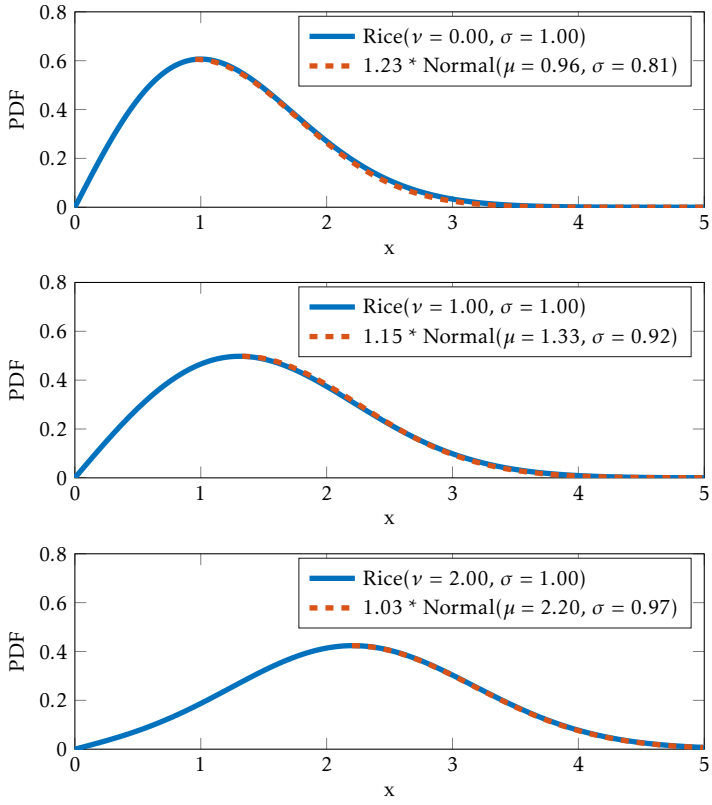

Figure 4.4: *PDF of the Rice distribution for different ν/σ ratios, and relation to a scaled half Gaussian distribution.*

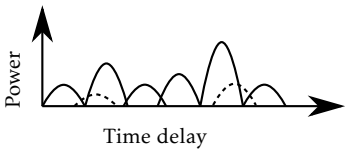

Figure 4.5: *Weak noise peaks being obscured by strong neighboring peaks. Obscured peaks are indicated by dashed lines.*

when $\nu/\sigma \approx 0$. This reflects that side lobes dominate the PDP error for high SNR, and that side lobes are practically insignificant for low SNR.

To suppress noise peaks and side lobes, the detection threshold is based on a Rice distribution, where a preferable probability of suppressing false detections is chosen.

4.3.5 Distribution Truncation

With a Rice distribution describing the noise peak amplitudes, the probability of a false detection of a noise peak with a certain amplitude can be expressed. The parameters required are amplitude variance σ^2 for noise peaks, and expected side lobe contribution ν from CIR components. However, these parameters are likely not sufficient. Due to the autocorrelation properties of the PRS, the PDP samples are not independent of each other but autocorrelated.

As the PDP noise peaks occur mainly as lobes with support over several PDP samples, there can be expected to exist overlapping lobes in the PDP. Therefore, if the noise lobes are assumed to follow a Rice distribution, but also overlap each other which is feasible as they are not perfectly separated, weak lobes will be overshadowed by stronger peaks. An illustration of this is found in Figure 4.5. Therefore, weaker noise peaks might be fewer than expected from the distribution.

This motivates a distribution which is truncated on the lower end at an empirically estimated amplitude, in order for at least the upper 50% of noise amplitudes to be approximated closely by the distribution. The reason the upper half of the distribution is of most importance is that the detection threshold should suppress noise effectively. Arguably, a threshold that only suppress 50% of all noise peaks, does not. However, if multiple PDP measurement occasions are considered, a more precise distribution might be motivated to avoid overestimating the noise probability and in turn reduce CIR peak detectability.

If lower amplitudes are also required to be reflected accurately by the distribution, another method than truncation should be applied. Although, in this case weak peaks with high probability of being noise is not required if the noise suppression is chosen to be sufficiently high.

4.3.6 Distribution Parameter Estimation

To estimate the Rice distribution parameter σ, several methods could be used. One method would be to find noise peaks and fit the amplitudes to a distribution. An alternative to this is to measure the variance of the received noise or PDP noise. As both of these reflects the noise level and should be independent of the PRS, the parameter σ should be directly proportional to them. In this study, the PDP noise variance σ_n is measured for parameter estimation.

4.4 Noise Suppression Thresholds

This section covers the derivation of detection and hearability thresholds. These thresholds are based on noise suppression probability. With the distribution of noise peak amplitudes derived in previous sections, the probability of noise peaks larger than certain amplitudes can be expressed as follows.

Definition 4.4 (Probability of noise peak amplitude). Let the measured variance of the PDP noise be $\hat{\sigma}_n$. Given a peak with expected side lobe amplitude ν from nearby peaks, the noise peak amplitude a is approximated to follow a truncated Rice distribution. Assume

$$a \sim \text{Rice}(\nu, \sigma), \text{ truncated by amount } \zeta \text{ at the lower end,} \tag{4.13}$$

$$\sigma = \beta\hat{\sigma}_n \tag{4.14}$$

where β and ζ are model parameters, chosen based on previous measurements. Given a peak, the probability $p_n(a)$ of a noise peak of amplitude a or larger can then be approximated by

$$p_n(a) = 1 - F(a; \nu, \sigma) \tag{4.15}$$

where F is the estimated Rice CDF.

This probability can be used to create a detection threshold for selection TOA candidates, and also a hearability threshold to determine which PDP measurements are too noisy to be useful. The selection of these thresholds is discussed in the following subsections.

4.4.1 Detection Threshold

Given the amplitude CDF for noise peaks, a detection threshold can be chosen with an arbitrary probability of false detections of noise peaks as TOA candidates. In this work, the following threshold definition is used.

Definition 4.5 (Detection Threshold). Assume $p_n(a)$ is the probability of a noise peak having amplitude a or larger. To have the probability $p_{\min}$ of false detection of a noise peak for each noise peak considered, the threshold $a_{\min}$ is used, where

$$p_n(a_{\min}) = p_{\min}. \tag{4.16}$$

4.4.2 Hearability threshold

A PDP measurement is only useful if CIR peaks are strong enough to be detected. This means the hearability of the PRS has to be determined for each PDP. For very low SNR, a noise peak will be the PDP maximum. In that case, the CIR peak amplitude cannot be considered strong compared to noise peaks, and noise suppression in the detection becomes challenging. Therefore, a hearability threshold to disregard noisy PDPs is required to allow proper detection.

A hearability threshold can be selected in the following way. Assume the PDP maximum is a noise peak of amplitude $a_{\max}$. In this case, all noise peaks have an equal or lower amplitude. The probability of a certain amplitude $a_{\max}$ can be expressed as

$$p_{n,\max}(a_{\max}) = [F(a_{\max}; \nu, \sigma)]^{N_n}, \tag{4.17}$$

where N_n is the expected amount of noise peaks in the PDP. Based on this, we can for a certain probability $p_{n,\max}$ calculate the expected distribution parameter σ, and in turn the PDP noise variance $\hat{\sigma}^2_{n,\max}$.

As the tolerated noise variance is proportionate to the PDP maximum $a_{\max}$, it is sensible to consider the normalized PDP with amplitudes between zero and one, which would allow for a constant hearability threshold among PDP measurements. Additionally, this allows the normalized PDP noise variance to act as a substitute to SNR. As σ_n is the ratio between PDP noise variance and PDP maximum, it is basically an inverse measurement of SNR, which is the ratio between signal and noise power. For the normalized PDP, the hearability threshold is defined as follows.

Definition 4.6 (Hearability Threshold). Assume the normalized PDP maximum is 1, and the probability of it being a noise peak is required to be $p_{n,\max}$ or lower. The PDP noise variance hearability threshold $\sigma_{n,\max}$ is given by

$$F(1; \nu_{\max}, \sigma_{\max}) = p_{n,\max}^{1/N_n}, \tag{4.18}$$

where $\nu_{\max}$ is chosen as an expected side lobe contribution, and $\sigma_{\max} = \beta\sigma_{n,\max}$ as before.

The threshold parameter $\nu_{\max}$ can be chosen for two different interpretations of the noise peak distribution. If noise peaks are assumed to influence neighboring peaks, $\nu_{\max}$ can be set to the side lobe contribution from neighboring peaks of standard deviation amplitude. Otherwise, if noise peaks are assumed to be approximately independent, $\nu_{\max} = 0$. In any case, if the PDP maximum is assumed to be large enough, $\nu_{\max}$ is approximately insignificant to the distribution and can be set to zero.

An empirical alternative is to measure the variance of normalized PDP noise and find a variance where most noisy measurements are disregarded. This alternative is easier and arguably better, as the model robustness do not influence the threshold. In any case, if the distribution model is used to derive a threshold, it would be tested and validated. Therefore, assume prior PDP noise variance measurements have been conducted and a hearability threshold $\sigma^2_{n,\max}$ selected to disregard most PDP measurements where a noise peak the maximum.

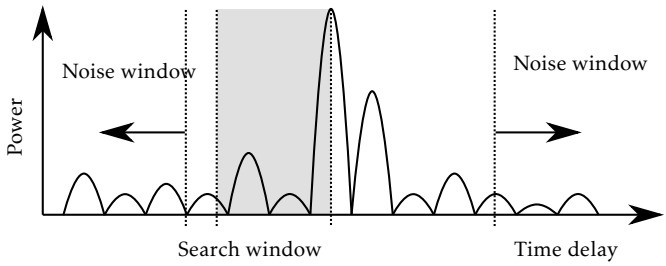

Figure 4.6: *Example search window and noise window for PDP measurements. The search window is indicated by gray background, and the noise window covers other time delay ranges, with a margin to the maximum peak.*

4.5 Search Window

To limit the amount of detected distant noise peaks, the detection should be limited to a search range nearby confident multipath peaks. A simple search window could begin at a confident CIR peak and cover a range of earlier samples. An illustration of a search window can be found in Figure 4.6. This window would limit the expected amount of noise peaks while covering most of the interesting peaks. The search window width should be based on empirical measurements of the TOA distribution of the strongest CIR peak, to assure that LOS TOA samples are included in most search windows. As the channel suffers from path loss, the strongest path is unlikely to be very much delayed compared to the LOS path.

One way of forming a search window is to consider the strongest peak as a confident CIR peak, and assume some knowledge about its TOA distribution in relation to the LOS CIR peak. Assuming the strongest CIR peak is restricted to a maximum delay from the LOS in most cases, the following definition is motivated.

Definition 4.7 (LOS Peak Search Window). Assume the PDP maximum occur at time delay $\tau_{\max}$. The LOS peak search window

$$\mathcal{S}_s = \{\tau_{\max} - N_{w,\text{LOS}},\ \ldots,\ \tau_{\max} - 1,\ \tau_{\max}\} \tag{4.19}$$

is the set of PDP samples under consideration when detecting peaks. The parameter $N_{w,\text{LOS}}$ should be chosen such that the search window covers the LOS sample for most cases, which might vary among BSs depending on environment.

4.6 Noise Window

As the detection model requires measuring the PDP noise variance, the CIR has to be excluded when calculating this. For this purpose, a noise window $\mathcal{S}_s$ is chosen. In this window only noise peaks are expected in order to reduce bias from CIR peaks. An example noise window is presented in Figure 4.6. The noise window is defined as follows.

Definition 4.8 (Noise Peak Window). The noise window

$$\mathcal{S}_n = \{0,\ 1,\ \ldots,\ N_\tau - 1\} \setminus \left\{\tau_{\max} - N_{n,pre},\ \ldots,\ \tau_{\max} + N_{n,post}\right\} \tag{4.20}$$

is the set of PDP samples under consideration when calculating noise statistics. N_τ is the number of time delays calculated for the PDP. The parameters $N_{n,pre}$ and $N_{n,post}$ should be chosen such that the noise window discards the CIR peaks surrounding $\tau_{\max}$ for most cases, which again might vary among BSs depending on environment.

5

Probabilistic TOA Candidate Detection Method

This chapter presents a Probabilistic TOA Candidate Detection method for detecting multiple TOA candidates that can be used in an OTDOA positioning algorithm. The method is based on peak detection in the PDP, with a detection threshold based on a SNR related measurement. This threshold is based on the measured noise level in the PDP, and estimates the probability of suppressing noise peaks. Then, each detected peak is regarded as a TOA candidate and is assigned a probability of being the first detected path. This probability is then used as candidate weight in the OTDOA positioning algorithm. Finally, the proposed method is compared to conventional methods.

The OTDOA positioning method proposed earlier requires a set of TOA candidates. In the previous chapter on the PDP properties, the probability of suppressing false detection of noise peaks was derived. For the candidate selection, this probability is first used to select a threshold for peak detection in the PDP, and then to assign each peak TOA candidate a probability of belonging to the first CIR component. As the purpose of the peak detection is to find the LOS peak, the first detected CIR component gives an estimate of the LOS component, with positive bias if the LOS is undetected.

5.1 Probabilistic TOA Candidate Detection

A Probabilistic TOA Candidate Detection algorithm is proposed as of Algorithm 5.1 on the next page. Short procedures are included as equations, but the complete procedures with motivation is found in the previous chapter.

Algorithm 5.1: Probabilistic TOA Candidate Detection.

1. Calculate the PDP

$$|R[\tau]| = \left| \sum_{i=0}^{N_w-1} x^*[i-\tau] y[i] \right|. \tag{5.1}$$

2. Find time delay $\tau_{\max}$ of maximum PDP amplitude $a_{\max}$

$$\tau_{\max} = \arg\max_{\tau} |R[\tau]|. \tag{5.2}$$

3. Normalize PDP amplitudes to be contained in the interval $[0, 1]$ by dividing all amplitudes by $a_{\max}$

$$R_{\text{norm}}[\tau] = |R[\tau]/a_{\max}| \tag{5.3}$$

4. Choose noise window

$$\mathcal{S}_n = \{0,\ 1,\ \ldots,\ N_\tau - 1\} \setminus \left\{\tau_{\max} - N_{n,pre},\ \ldots,\ \tau_{\max} + N_{n,post}\right\} \tag{5.4}$$

in which to measure noise statistics.

5. Calculate PDP noise variance $\hat{\sigma}_n^2$ using R_{norm} at time delays $\mathcal{S}_n$.

6. Compare $\hat{\sigma}_n^2$ to a chosen hearability threshold $\sigma_{n,max}^2$. If $\hat{\sigma}_n^2 > \sigma_{n,\max}^2$, stop and disregard the PDP measurement.

7. Calculate a peak amplitude threshold $a_{\min}$ based on $p_{\min} = 1 - F(a_{\min}; \nu, \sigma)$ for noise suppression, where $\nu = 0$ and $\sigma = \beta\hat{\sigma}_n$.

8. Choose CIR search window

$$\mathcal{S}_s = \{\tau_{\max} - N_{w,\text{LOS}},\ \ldots,\ \tau_{\max} - 1,\ \tau_{\max}\}. \tag{5.5}$$

9. Detect peaks $\mathcal{P}$ in R_{norm} at time delays $\mathcal{S}_s$, with peak amplitude $a_k > a_{\min}$ at time delay τ_k.

10. For each peak p_k in $\mathcal{P}$, calculate adjusted threshold $a_{\min,k}$ by accounting for side lobes from other detected peaks by using ν given by

$$\nu_{p_k}^2 = \sum_{p \in \mathcal{P},\ p \neq p_k} a_{\text{lobe},p}^2(|\tau_p - \tau_{p_k}|) \tag{5.6}$$

11. Return $\mathcal{P}$ where $a_k > a_{\min,k}$ as CIR peak candidates.

5.2 TOA Candidate Probability

In this section, the probability of each TOA candidate being the first detected path is proposed. The probability considers the probability of suppressing noise and an expected distribution of CIR peaks.

The peak detection in PDP can be interpreted as a ML estimator of TOA, as the PDP approximates the CIR which in turn can be interpreted as a (scaled) PDF of the TOA. This interpretation of the PDP as a PDF for TOA is a good first step, and allows detection of multiple TOA hypothesis. As a second step, it should be noted that it is seldom interesting to consider peaks after the strongest for TOA candidates. This is because the strongest peak need to be a CIR peak in most cases, as the signal otherwise would be practically undetectable and the PDP dominated by noise peaks. The peak order dependency in the direct PDP to PDF interpretation motivates further modeling to support multiple hypotheses with peak order awareness.

Given a set of TOA candidate peaks, the probability of each being a CIR peak is required for the ML estimation. As a continuation on the noise suppression probability, the probability of each detected peak being a CIR peak is expressed. If the amplitude and time delay distribution of CIR peaks are unknown, but the amplitude of CIR peaks is assumed to be relatively strong compared to noise peaks, a simplified CIR peak probability can be assigned. The CIR peak probability used in this thesis is discussed in the following subsections.

5.2.1 Distance Penalty

As the probability of detecting a noise peak increases the more peaks are considered, it is feasible to consider a probability penalty for peaks based on their distance to certain CIR peaks. An approach to apply penalty to peaks early in the search window is to consider the cumulative probability of detecting a noise peak. For a detected peak, the probability of detecting a noise peak increases the more PDP samples have been considered. Therefore, the assigned probability for a peak could include this by approximating the probability of detecting a noise peak with this amplitude over the searched range.

If the search begin at the strongest peak, each additional sample considered would cause the probability of noise to increase. Effectively, the probability of detecting a CIR peak would decrease exponentially with the distance to the strongest peak. This is essentially a variant of an exponential distribution model for the NLOS delay, which is commonly used according to [4].

Another factor to consider is the distribution of CIR peaks. If the CIR is assumed to follow an exponential distribution as in [4], this should be reflected in the probability. Accounting for both noise suppression and CIR distribution, the following probability assignment is used.

Definition 5.1 (Probability of CIR peak). The probability $\hat{p}_n(a)$ of suppressing all noise peaks of amplitude a or smaller over a range of d samples is

$$\hat{p}_n(a) = [p_n(a)]^{\rho d} \tag{5.7}$$

where $\rho \in [0, 1]$ is the expected number of noise peaks per sample. The probability of being a CIR peak is estimated as

$$p_{\text{CIR}}(a) = \hat{p}_n(a)[p_n(a)]^{\alpha_d d} = [p_n(a)]^{\hat{\alpha}_d d} \tag{5.8}$$

where $\hat{\alpha}_d = \alpha_d + \rho$, and α_d is a factor to represent an expected exponential distribution of NLOS bias in detected peaks. For CIR peaks to be assumed equally likely in the whole search window, $\alpha = 0$ represents no distance penalty from NLOS bias distribution. Also, the calculated exponent $\hat{\alpha}_d d$ should be at least 1 to avoid overestimating CIR peak probabilities.

5.2.2 Distance to Uncertain Peaks

To assign the probability proposed, a distance measure d for each peak candidate is required. As the strongest peak is a confident CIR peak, the separation of each peak and the strongest can be used. However, if there is several strong peaks preceding the strongest, this distance measure is most likely too large. Instead, all trailing peaks could be considered as uncertain CIR peaks when the distance to a confident CIR peak is calculated. Therefore, in this study the expected distance to a CIR peak is used to calculate the CIR probability. The expected distance is given as follows.

Definition 5.2 (Expected distance to previous CIR peak). Assume an ordered set of K peaks have been detected, with a probability of being a path $p_{\text{CIR},k}$, $k = 1, 2, \ldots, K$, where $k = 1$ indicates the first peak and $k = K$ the last. For the strongest peak, assume $p_{\text{CIR},K} = 1$. Let the distance from peak k to peak $k + 1$ be d_k. The expected distance to a CIR peak $\hat{d}_k$ is

$$\hat{d}_k = d_k + (1 - p_{\text{CIR},k+1})\hat{d}_{k+1}. \tag{5.9}$$

As the last peak is a confident CIR peak, we have $d_K = 0$.

5.2.3 Consecutive TOA Candidates

As stated earlier, with multiple TOA candidates, each candidate have to be assigned a weight. This weight should reflect the probability of being the best estimate. For this purpose, the probability of each peak being the first CIR peak is used. This is reasonable as the first detected CIR peak always is a better estimate than later peaks. This probability of being the first CIR peak can be expressed in terms of the CIR probability. For the first detected peak, the probability of it being the first detected CIR peak is simply the probability of being a CIR peak. For following peaks, the probability is dependent on preceding peaks being noise. The probability used for the candidate weight can be expressed as follows.

Definition 5.3 (Probability of first CIR peak). Assume an ordered set of K peaks have been detected, with probability of being CIR peaks $p_{\text{CIR},k}$, $k = 1, 2, \ldots, K$, where $k = 1$ indicates the first peak and $k = K$ the last. The probability $p_{\text{first},k}$ of

being the first CIR peak is

$$p_{\text{first},k} = \left(\prod_{j=1}^{k-1} (1 - p_{\text{CIR},j}) \right) p_{\text{CIR},k}. \tag{5.10}$$

The probabilities sum to one as the last peak is the strongest and also a certain CIR peak.

5.2.4 Probability Assignment

To calculate the probability weight of each TOA candidates, the following algorithm is proposed based on the discussion earlier in this section. The probability $p_n(a)$ is calculated as of Definition 4.4 on page 27. An illustrating example of the probability weights can be found in Figure 5.1 on the next page.

Algorithm 5.2: TOA candidate probability assignment.

Assume an ordered set $\mathcal{P}$ of K peak candidates have been detected, where $k = 1$ indicates the first peak and $k = K$ the last.

1. Calculate the probability of each candidate being a CIR peak as

$$p_{\text{CIR},k}(a) = [p_n(a_k)]^{\hat{\alpha}_d \hat{d}_k} \tag{5.11}$$

where $\hat{\alpha}_d$ is a distance penalty factor and

$$\hat{d}_k = d_k + (1 - p_{\text{CIR},k+1}) \hat{d}_{k+1} \tag{5.12}$$

is the expected distance to a CIR peak, where d_k is the distance from peak k to peak $k + 1$, and $d_K = 0$ for the last peak.

2. The probability $p_{\text{first},k}$ of being the first CIR peak is estimated as

$$p_{\text{first},k} = \left(\prod_{j=1}^{k-1} (1 - p_{\text{CIR},j}) \right) p_{\text{CIR},k}. \tag{5.13}$$

3. Return $p_{\text{first},k}$ as the weight for each TOA candidate.

5.3 Relation to Conventional Methods

A quick reflection on the validity of the Probabilistic TOA Detection model can be done by relating to the *Peak-to-Average-Power Ratio* detection. Based on the PAPR detection rule, the PDP mean is used for threshold detection of peaks.

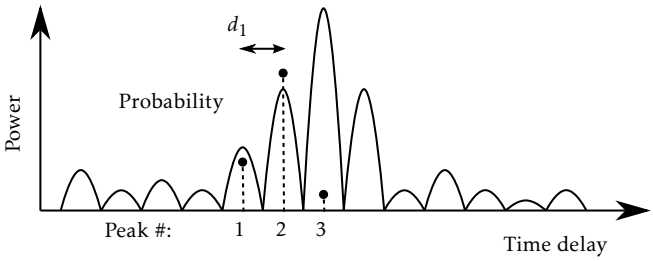

Figure 5.1: *Example probability assignment for a set of PDP peaks. The probability weight of each peak is indicated by a dashed stem ending with a dot. The distance between the first detected peaks is also indicated, which is used in the probability calculations. The strongest peak is given a very low probability due to a preceding peak which is strong compared to noise peaks.*

Only peaks with a PAPR ratio over a threshold is considered, and from these the strongest peak is picked. The threshold is essentially a hypothesis test for a certain error probability. The proposed Probabilistic TOA Candidate Detection algorithm can therefore be seen as a generalization of the PAPR criterion, but with a noise sensitive threshold and multiple candidates.

By considering peaks, it can also be compared to *Peak-to-Mean-Envelope-Power Ratio* (PMEPR) detection. In signal theory, the peak amplitude of a signal is said to be contained within the envelope. Focusing on the peaks of the PDP can therefore be interpreted as studying the PDP envelope. In this case, the signal is the superposed PRS autocorrelation sinc functions, and by studying the peaks, the autocorrelation properties of the PDP should be less emphasized than if every sample were studied.

Another method is to select the first peak with amplitude above half that of the maximum peak, as done in [23]. This reduces the probability of wrongfully selecting a side lobe if only the PAPR criterion is considered. However, the half-maximum threshold essentially have to be roughly equivalent to the noise sensitive threshold for low SNR, as it otherwise would select the wrong peak too often for low SNR measurements. Therefore, the constant threshold can be seen as a worst-case threshold independent of the SNR.

6

Simulation Scenario Setup

This chapter presents the simulation setup and scenario parameters used to obtain PDP measurements, and the chosen parameters for the TOA detection and OTDOA positioning.

6.1 Simulation Environment

The measurement data are obtained from a radio channel simulator provided by Ericsson. By using simulations, the results can be compared to other studies using the same simulation parameters. To make the results comparable to other studies, the scenario and simulation model are based on the 3GPP agreement TR37.857 [26]. Information on the channel model used in the simulations can be found in [8, App.B].

In short, the simulator models an urban scenario with outdoor BSs and indoor UEs. The location and velocity of the UEs are considered when calculating the propagation channel. The propagation accounts for large scale parameters such as shadowing and path loss, and multi path parameters including power, delay and angles. Finally, using the scenario and propagation parameters, a set of CIR coefficients for each measurement is created.

The simulation scenario is based on a 3GPP agreement scenario for indoor UEs and outdoor BSs, TR37.857 [26]. In the studied scenario, there are 7 macro sites with 3 cells each. The sites are located in a hexagonal grid with *Inter-Site Distance* (ISD) 500m. The simulation scenario consists of 70 indoor UEs, each measuring 8 PRS occasions from the 21 BSs. An illustration of the deployment is shown in Figure 6.1 on the following page. The BS locations for each UE are adjusted so that all UEs are surrounded by BSs, as described in [12].

The study only considers indoor users and outdoor macro BS. This approach is motivated as the positioning accuracy for TDOA based methods are worst in en-

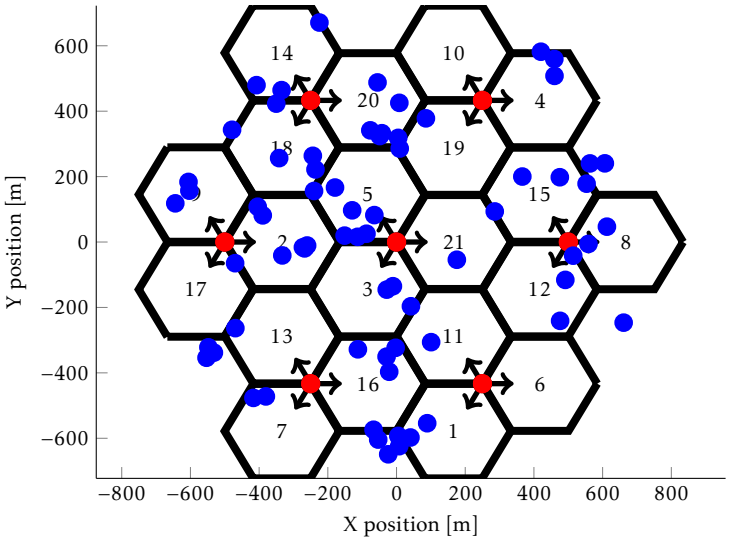

Figure 6.1: *Deployment scenario with UEs marked as blue dots in numbered RAN serving cells, and BSs transmitting PRSs in directions indicated by arrows. In the simulations, a wrapping method is applied to the BSs positions so that all users are surrounded by BSs.*

vironments with large fading and NLOS components dominating the CIR, which is the case for indoor users. Also, only 2D locations are estimated; the elevation coordinate evaluated for results is the true elevation of each UE. A list of parameters for the scenario is presented in Table 6.1 on the next page and Table 6.2 on the facing page.

6.2 Detection Parameters

In this section, the parameters used in the timing and positioning method are presented. For a full reference, see Table 6.3 on page 41. The search window was selected to cover a range of 51 samples before the strongest peak, which equals 500m. For the studied scenario, this included the LOS path for 98% of the PDPs which were above the hearability threshold. The noise window disregarded 102 samples on both side of the strongest peak, corresponding to 1000m.

The hearability threshold parameters were chosen as $p_{n,\max} = 0.001$, the probability of not disregarding noisy PDPs, which resulted in the hearability threshold for PDP noise variance $\sigma_{n,\max} = 0.114$. For the peak detection, the probability of detection of noise peaks were selected as $p_{\min} = 0.1$ for the multiple TOA candidate case, and $p_{\min} = 0.001$ for the single first peak case.

Table 6.1: *Scenario deployment parameters.*

Parameter	Value
Layout	Hexagonal grid, 3 sectors per site, 7 Macro sites, ISD = 500m
System BW per carrier	10MHz
Carrier frequency	2.0GHz
Carrier number	1
Total BS TX power	46dBm
Distance-dependent path loss	3D-UMa (Table 7.2-1 in TR36.873 [25])
Penetration	20dB + $0.5d_{in}$, $d_{in} \sim$ uniform$[0, \min(25, d)]$ for each link
Shadowing	3D-UMa (Table 7.3-6 in TR36.873 [25])
Antenna pattern	3D (TR36.819 [5])
Antenna height	25m+α, $\alpha \sim$uniform$[-5, 25]$
UE height	$hUT = 3(n_{fl} - 1) + 1.5$m, $n_{fl} \sim$ uniform$[1, N_{fl}]$, and $N_{fl} = 8$
Antenna gain + connector loss	17dBi
Antenna gain of UE	0dBi
Fast fading channel between eNB and UE	3D-UMa (Table 7.3-6 in TR36.873 [25])
Antenna configuration	2Tx2Rx in DL, Cross-polarized.
Number of buildings per macro cell geographical area	1
Numbers of floors per building	$N_{fl} = 8$
UE dropping	2/3 UEs randomly and uniformly dropped within the clusters, 1/3 UEs randomly and uniformly dropped throughout the macro geographical area. 100% of UEs are indoor.
Radius for UE dropping in a cluster	70m
Minimum distance (2D distance)	Macro–UE: 35m; cluster center–cluster center: 100m
UE noise figure	9dB
UE speed	3km/h
Network synchronization error	Perfectly synchronized.
UE calibration error	Perfectly synchronized.

Table 6.2: *Scenario PRS parameters.*

Parameter	Value
Cyclic prefix	Normal
Number of consecutive PRS subframes	1
Number of positioning occasions	8
PRS periodicity	160ms
PRS bandwidth	10MHz
RBs allocated for PRS	50
PRS muting	on for main scenario, off for worst-case comparison scenario.
Sampling frequency	30.72MHz

6.3 GM Parameters

The selection of parameter values for the GM used in the ML positioning is an important configuration step. To constrain the complexity of the optimization problem, the amount of mixture components K_i for the GM should be given a maximum count. This count should be based on the expected information gain from additional TOA candidates. A similar restriction should be applied to the number of reported BSs N, as the gain from additional BSs also decrease.

The noise mixture means m_{i,k_i} are preferably chosen as the TOA of each detected peak, potentially with an offset to account for expected NLOS bias. If detectability of early peaks are good, and the standard deviation σ_{i,k_i} is of similar order as an expected NLOS bias, an offset might yield only limited accuracy improvement and is therefore not considered in this study. Furthermore, as the positioning is done using differences, a constant offset would not improve the positioning accuracy. Therefore, only the TOA candidates τ_{i,k_i} are considered which gives the measurement noise mixture means

$$m_{i,k} = \tau_{i,k_i} - t_i \tag{6.1}$$

which yields the residuals

$$r_{i,k_i} = \tilde{t}_i - \tau_{i,k_i} \tag{6.2}$$

where $\tilde{t}_i$ is the expected TOA for the position.

The GM variance σ^2_{i,k_i} should account for the measurement error and the detectability of nearby peaks. The measurement error could simply be directly linked to the peak width, and the detectability of other peaks depends on the noise level. Assuming the PDP peaks approximately match a $sinc$ function main lobe, other peaks are hard to detect in the near vicinity. Therefore, a choice of σ_{i,k_i} could be to approximate the peak shape in the GM for high SNR. By using the rule of 2σ to fit the sinc function main lobe of the PRS autocorrelation with a Gaussian function, the variance is given as

$$2\sigma_{i,k_i} = w/2, \tag{6.3}$$

where w is the width of the main lobe. This width is given by

$$w = \frac{2f_s}{\mathrm{BW}_{\mathrm{RB}} N_{\mathrm{RB}}} \tag{6.4}$$

where $\mathrm{BW}_{\mathrm{RB}} = 180\mathrm{kHz}$ is the bandwidth of a RB, N_{RB} is the number of RBs allocated for the PRS, and f_s is the sampling frequency.[1] The factor 2 is to account for the lobe width on both sides of origin. This GM variance assumes that the side lobes do not significantly affect the detectability of nearby peaks. In this study, the positioning accuracy improved when the variance increased up to the 2σ value, but beyond that no significant improvement were detected.

[1] This main lobe width results in zero autocorrelation for all non-zero integer sample lags when the sampling frequency and PRS bandwidth are equal.

Table 6.3: *Method parameters.*

Parameter	Value	Description
β	1.73	$\hat{\sigma}_n$ scale factor for Rice parameter σ
ζ	0.33	Rice distribution truncation amount
$p_{\min}$	0.1	probability of detection of noise peak
$p_{n,\max}$	0.001	probability of not disregarding noisy PDP
$\sigma_{n,\max}$	0.114	threshold PDP noise variance for disregarding PDP
$N_{w,\text{LOS}}$	51	number of samples before $\tau_{\max}$ for $\mathcal{S}_s$
$N_{n,pre}$	102	number of disregarded samples before $\tau_{\max}$ for $\mathcal{S}_n$
$N_{n,post}$	102	number of disregarded samples after $\tau_{\max}$ for $\mathcal{S}_n$
$N_{\max}$	14	maximum number of BSs included in positioning
$\hat{\alpha}_d$	2	candidate probability factor for distance penalty
α_σ	1	coefficient for GM variance noise dependency

To reflect the detectability of peaks being dependent on the SNR, a linear increase of σ_{i,k_i} based on the measured PDP noise variance $\hat{\sigma}^2_{n,i}$ is used. This linear dependency is modeled as

$$\sigma_{i,k_i} = (1 + \alpha_\sigma \frac{\hat{\sigma}_{n,i}}{\sigma_{n,\max}}) \cdot w/4 \tag{6.5}$$

where $\sigma_{n,\max}$ is the hearability threshold for PDP noise variance and α_σ is a constant coefficient. This model effectively increase the GM variance α^2_σ times when the PDP noise variance increase from zero to the accepted maximum.

6.4 Evaluation Method

There are two distinct options to applying the GM PDFs for a ML estimation. For each cell, one GM component can be evaluated at a time, and the resulting positions weighted together [10, 15]. Otherwise, the complete GM can be evaluated at once, resulting in a more complex target function with possibly several local optima. To calculate the position, the Gauss-Newton algorithm could be used [10]. Other applicable algorithms are grid search and Monte-Carlo sampling, which can also produce a heat map of the position likelihoods of some cases to illustrate the estimation accuracy.

In this study, the complete GM is evaluated at once, and the position is estimated by evaluating the likelihood function in a grid search. Given that the number of considered TOA candidates for each GM is kept restricted, the computational complexity should not be a problem. Unlike Gauss-Newton, a grid search do not require the derivation of a gradient, and allows producing heat maps for accuracy illustration purposes.

The grid search is done in several iterations with increased grid resolution in every step. An illustration of the grid search can be seen in Figure 6.2 on the following page. The search is explained in text here, and in Algorithm 6.1.

Table 6.4: *Grid search parameters.*

Parameter	Value	Description
$\mathbf{x}_{e,1}$	(0, 0)	initial grid center
$d_{grid,1}$	$4 \cdot c/f_s \approx 39$m	initial grid point distance
$d_{grid,\min}$	$1/8 \cdot c/f_s \approx 1.22$m	target grid point distance
$N_{grid,1}$	36	initial number of points in grid side
$N_{grid,iter}$	4	number of points in grid side for iteration

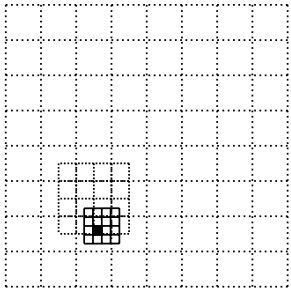

Figure 6.2: *Grid search in an iteration with increasing resolution and decreasing search area, with the ML position indicated by a filled box. Three iteration steps are displayed.*

First, a low-resolution grid over the full simulation area is searched. The first grid spans is centered on origin, is square and spans 1370m across, which covers all UEs. The initial resolution is set to be 4 times the sampling resolution, about 39m. The following iteration are centered on the ML position from the previous iteration, have half the grid point distance, and spans 4 grid points across. The parameters for the grid search can also be found in Table 6.4.

This method yields a poor accuracy for the early iterations, but limits the search and increases the accuracy with each iteration. By letting the next grid iteration cover an area around the current ML position, the distance from the true ML position is decreased by each iteration, assuming there is only a single dominant local ML optimum.

Algorithm 6.1: Iterative Grid Search

Assume a set of TOA candidates have been detected for N BSs. To estimate the UE position, the following steps are performed.

1. Specify an initial grid, and denote the iteration index $m = 1$ for the initial step. The grid center is $\mathbf{x}_{e,m} = \mathbf{x}_{e,1}$, the grid point distance is $d_{grid,m} = d_{grid,1}$, and the grid side contain $N_{grid,m} = N_{grid,1}$ points.
2. Calculate the GM constants according to Algorithm 6.2 on the following page.
3. For each grid point $\mathbf{x}$, calculate the position likelihood according to Algorithm 6.3 on page 45. Set the position estimate $\mathbf{x}_{e,m+1}$ to the ML position.
4. If $d_{grid,m} \leq d_{grid,\min}$, stop and return the position estimate $\mathbf{x}_{e,m+1}$.
5. Set $d_{grid,m+1} = d_{grid,m}/2$ and set the grid center to $\mathbf{x}_{e,m+1}$. Set the grid side to contain $N_{grid,m+1} = N_{grid,iter}$ points. Repeat the algorithm from step 3 using iteration index $m + 1$.

Algorithm 6.2: Calculate GM constants

The BSs are indexed by $i = 1, \dots N$, and the TOA candidates are indexed by $k_i = 1, \dots, K_i$ where K_i is the number of TOA candidates for BS i. The mixture weights of the TOA candidates are denoted p_{i,k_i}.

1. For each set of TOA candidates, calculate the GM variance

$$\sigma_{i,k_i} = (1 + \alpha_\sigma \frac{\hat{\sigma}_{n,i}}{\sigma_{n,\max}}) \cdot w/4 \tag{6.6}$$

where $\hat{\sigma}_{n,i}$ is the measured PDP noise variance for BS i, $\sigma_{n,\max}$ is the hearability threshold for PDP noise variance, and w is the width of the main lobe of the PRS autocorrelation, given by

$$w = \frac{2f_s}{\mathrm{BW}_{\mathrm{RB}} N_{\mathrm{RB}}} \tag{6.7}$$

where $\mathrm{BW}_{\mathrm{RB}} = 180$kHz is the bandwidth of a RB, $N_{\mathrm{RB}} = 50$ is the number of RBs allocated for the PRS, and $f_s = 30.72$MHz is the sampling frequency.

2. For each combination of TOA candidates[2] among the N BSs, calculate the GM constants

$$c_{k_1,k_2,\dots,k_N} = (2\pi)^{-\frac{N-1}{2}} \frac{\prod_{i=1}^{N} p_{i,k_i}}{\sqrt{\sum_{i=1}^{N} \left\{ \prod_{j=1, j\neq i}^{N} \sigma_{j,k_j}^2 \right\}}}, \tag{6.8}$$

$$\sigma^2_{k_1,k_2,\dots,k_N} = \frac{\prod_{i=1}^{N} \sigma_{i,k_i}^2}{\sum_{i=1}^{N} \left\{ \prod_{j=1, j\neq i}^{N} \sigma_{j,k_j}^2 \right\}}. \tag{6.9}$$

Algorithm 6.3: Calculate position likelihood

This calculation use the same notation as Algorithm 6.2 on the facing page. The TOA candidates are denoted τ_{i,k_i}.

1. For each TOA candidate, calculate the residual

$$r_{i,k_i} = \tilde{t}_i - \tau_{i,k_i} \tag{6.10}$$

where $\tilde{t}_i$ is the expected TOA for the evaluated UE position (also expressed in sample periods), given by

$$\tilde{t}_i = \left(\sqrt{(x - x_i)^2 + (y - y_i)^2} \right) f_s / c \tag{6.11}$$

where (x, y) is the evaluated grid position, (x_i, y_i) is the position of BS i, f_s is the sampling frequency, and c is the speed of light.

2. For each combination of TOA candidates among the N BSs, calculate the GM variables

$$\mu_{k_1,k_2,\ldots,k_N} = \frac{\sum_{i=1}^{N} \left\{ \left(\prod_{j=1, j\neq i}^{N} \sigma_{j,k_j}^2 \right) r_{i,k_i} \right\}}{\sum_{i=1}^{N} \left\{ \prod_{j=1, j\neq i}^{N} \sigma_{j,k_j}^2 \right\}}, \tag{6.12}$$

$$\lambda_{k_1,k_2,\ldots,k_N} = \frac{\sum_{i=1}^{N} \left\{ \left(\prod_{j=1, j\neq i}^{N} \sigma_{j,k_j}^2 \right) r_{i,k_i}^2 \right\}}{\sum_{i=1}^{N} \left\{ \prod_{j=1, j\neq i}^{N} \sigma_{j,k_j}^2 \right\}}. \tag{6.13}$$

3. Calculate the likelihood for the position, given by

$$p(\tilde{t}_{N1}, \ldots, \tilde{t}_{21}) = \sum_{k_N}^{K_N} \cdots \sum_{k_2}^{K_2} \sum_{k_1}^{K_1} c_{k_1,k_2,\ldots,k_N} \cdot \exp\left(\frac{\mu_{k_1,k_2,\ldots,k_N}^2 - \lambda_{k_1,k_2,\ldots,k_N}}{2\sigma_{k_1,k_2,\ldots,k_N}^2} \right). \tag{6.14}$$

7

Results

In this chapter the results of the proposed method are presented. First, the positioning accuracy results for the proposed method and single TOA candidate variations are covered. Then, the timing accuracy for the detected TOA candidates is demonstrated. Finally, results related to the noise model regarding both the relative noise variance and the noise peak amplitude distribution are shown.

The results are based on 70 UEs performing 8 PRS measurement occasions each for 21 cells. For the time estimation, this equals 10290 PDP measurements, and for the positioning, 560 position estimates. For each received PDP with a noise variance below $\sigma_{n,max} = 0.114$, the peak detection algorithm was applied. This hearability threshold corresponds to wrongly keeping 0.1% of pure noise measurements, according to the estimated noise peak distribution. As the share of unhearable cells was high for the non-muted scenario, the threshold was chosen to be low.

7.1 Positioning Results

This section presents the position estimation results for the TOA candidates. A visualization of the ML method that was used can be seen in Figure 7.1 on page 49, where a UE measurement occasion have been evaluated and resulted in a ML estimate.

The overall accuracy results are presented in Figure 7.2 on page 49 and Table 7.1 on the next page. The position errors for all UEs are presented in two metrics: the error of each separate positioning occasion and the error of the positioning occasion among eight with the highest likelihood (denoted ML). For the case of multiple peaks, the noise suppression threshold was set to 90%. For single peak performance, the threshold was 99.9%. For the non-muted case, the ML error was not significantly lower than that of the separate occasions. The accu-

Table 7.1: *Positioning error CDF. Errors in meters are presented for the proposed method, and conventional method selecting the first peak exceeding half the maximum peak. The errors for both single positioning occasions and the occasion with the highest likelihood value among eight, are included.*

CDF	.50	.70	.80	.90	.95	.99
Single positioning occasion						
Study, multiple peaks	11	16	20	43	75	155
Study, single peak	13	21	30	54	78	161
Constant threshold (half max)	25	38	54	86	115	170
ML positoning occasion among eight						
Study, multiple peaks	7	12	15	16	22	101
Study, single peak	7	13	15	22	32	101
Constant threshold (half max)	13	18	28	45	63	148

racy is similar to the muted scenario, but with about 20% lost UEs. This is seen in Figure 7.3 on page 50.

The distribution of number of detected cells is presented in Figure 7.4 on page 50, and can be seen to provide redundancy in most cases for the muted scenario. However, for the non-muted scenario, the hearability of the PRS was lower, and about 7 cells were detected on average. The share of occasions with at least 3 correctly detected cells were less than 90%, which means many UEs could not be positioned at all.

7.2 Peak Detection

In this section, the timing accuracy of the detected TOA candidates is presented. Three TOA detection thresholds are considered. As a baseline, only the strongest PDP peak is reported. Still using a single candidate, the first PDP peak with an estimated noise probability below 0.1% is used. Finally, allowing multiple reported TOA candidates, all peaks in the search window with noise probability below 10% are considered.

The errors for the first detected peak, the best peak in terms of error, and the strongest peak are stored. The first and strongest peaks give a hint of what search window have been used, as the first peak is highly dependent on the threshold level which suppresses noise, and the strongest peak is the last peak to consider. The best TOA peak is included to give an optimistic hint of what additional information can be expected to be reported with the multiple candidates method.

The detected peak count for some variations in the threshold is presented in Figure 7.6 on page 52. This measurement gives some information about how much data is required to approach a specific TOA error. For high thresholds, the first detected peak is the best estimate in almost all cases.

As can be seen in Figure 7.5 on page 51, for a sufficiently high threshold, a

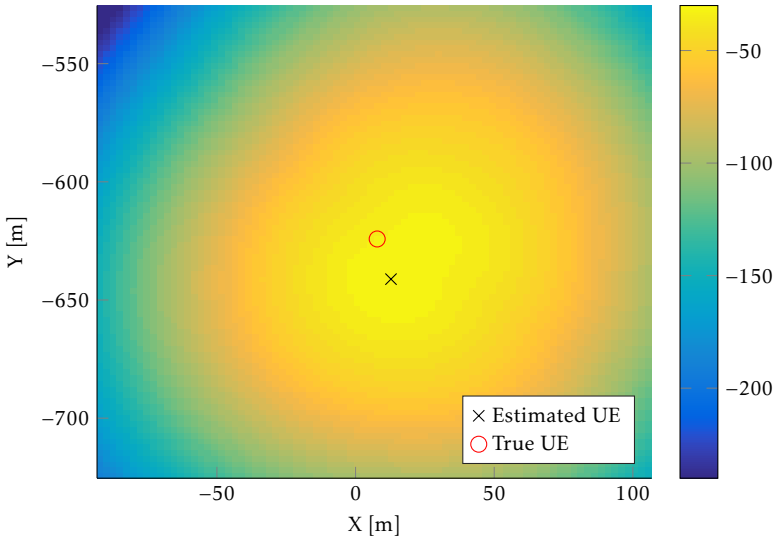

Figure 7.1: *Heatmap of the log-likelihood for evaluated positions in a surrounding area of an estimated ML position. The likelihood can be seen to reach its maximum close to the true position and be void of other local optima. The distance error is 18 m, using 30 peaks detected over 14 cells.*

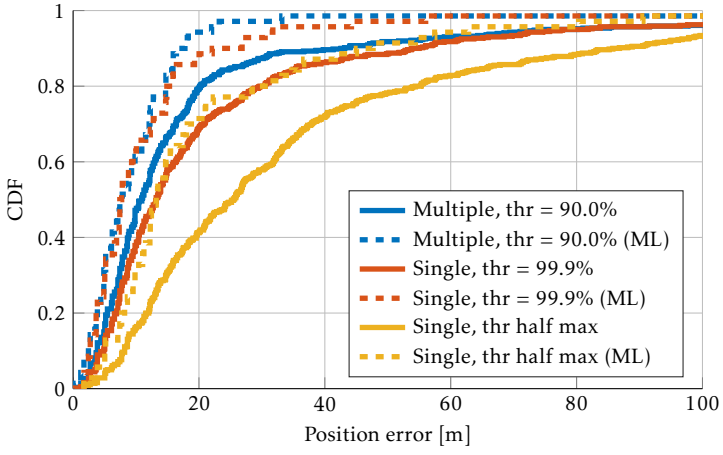

Figure 7.2: *Position error CDF. By using a SNR sensitive threshold instead of half the maximum amplitude as threshold to detect the first peak, the error is greatly reduced for the single TOA candidate case. The error is further reduced when using a lower threshold and allowing multiple candidates. The gain of multiple candidates is diminished as several measurement occasions are considered and the ML position among all occasions is taken as the estimate.*

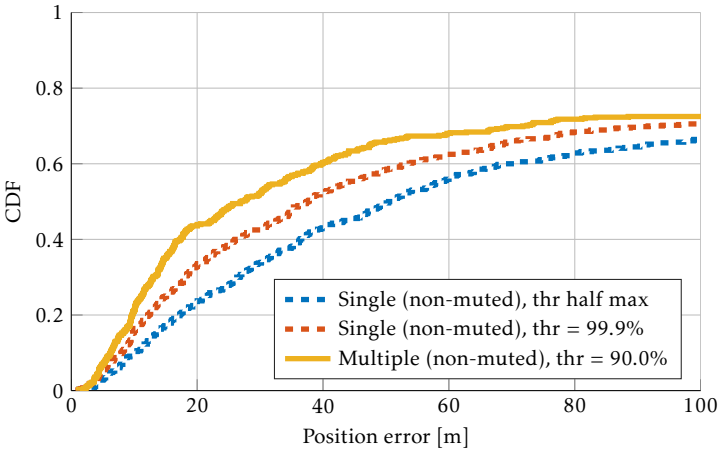

Figure 7.3: *Position error for the non-muted scenario. The proposed method with multiple TOA candidates detected by a relatively low threshold achieve higher accuracy than when only a single candidate is considered. The share of UEs unable to be positioned approximately corresponds to the amount of occasions with less than 5 detected PRS cells.*

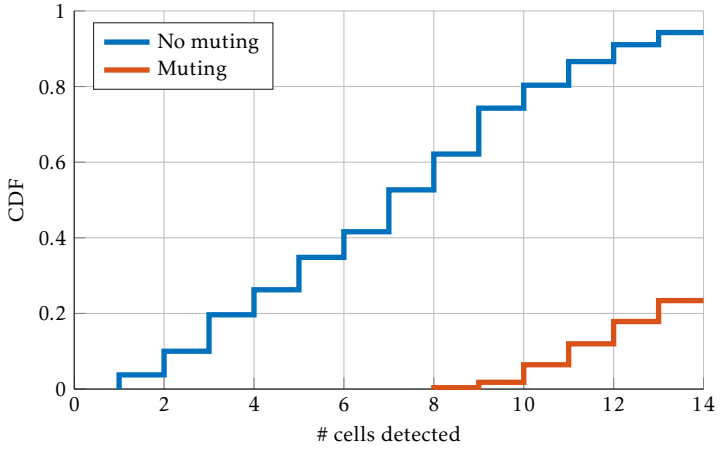

Figure 7.4: *Number of detected cells. Both the scenario with PRS muting and without are presented. For the non-muted scenario, about 20% of UEs could only detect 3 cells or less. The study limited the positioning to only use the strongest 14 cells.*

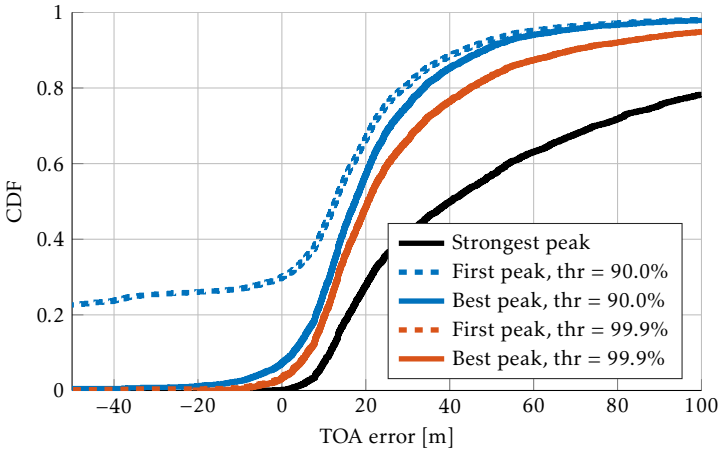

Figure 7.5: *TOA error for detected key peaks. The detection threshold is based on the Rice distribution approximated from the PDP noise variance, and chosen to suppress a certain percentage of noise peaks. In the figure two thresholds are present; a high threshold suppressing practically all noise peaks, and a low thresholds detecting earlier CIR peaks but also some noise peaks. The distribution of the strongest peak is included as an indication of the search range.*

multipath component earlier than the strongest can be found in many cases while still suppressing false detections. The first peak coincide with the best peak in this case. For a lower threshold, noise suppression is worse but weaker multipath components can be detected. This can clearly be seen in Figure 7.5, where the first detected TOA also include false noise peaks before the LOS component.

The case without muting of PRS signals yields very similar results as the muted scenario, as the hearability and detection thresholds are SNR sensitive. Therefore, measurements with too low SNR are disregarded, and among those left the TOA detection performance is practically the same, as the interference can be regarded as noise in this case.

7.3 Noise Peak Assumption Validation

For validation of the distribution of noise peak amplitudes, the amplitudes of peaks outside of a 1000m trailing interval from the true TOA were measured for all measurement occasions. The measured noise amplitude CDF was then compared to the estimated CDF. These peak amplitude distributions are shown in Figure 7.7 on page 53. In the figure, the noise peak amplitude for three different noise variances σ_n are shown for the case of very low side lobe contribution. The blue curves with $\sigma_n = 0.04$ approximately correspond to SNR −2dB, the red curves with $\sigma_n = 0.08$ have about −8dB, and the yellow curve about −11dB. For the muted scenario, many detected cells had SNR above 0dB, which means their

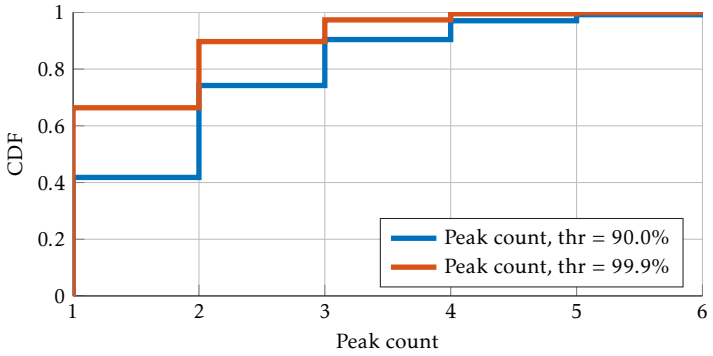

Figure 7.6: *Detected peak count. The peak count increases when the threshold is decreased, as additional weaker CIR peaks and some noise peaks are detected. For the 99.9% threshold, 1.5 peaks were detected on average, and for the 90% threshold, 2.0 peaks.*

distribution CDFs should be expected left of the blue curve.

The estimated Rice distribution was given by

$$\text{Rice}(\sigma = \beta\hat{\sigma}_n, \nu) \tag{7.1}$$

where $\hat{\sigma}_n^2$ is the PDP noise variance, ν is the root of the sum of squared expected amplitudes of side lobes, $\beta = 1.73$, and the distribution was truncated by $\zeta = 0.33$ on the lower end.

The relation between the normalized PDP noise variance and SNR is presented in Figure 7.8 on the facing page. The variance is shown as standard deviation, and at three different percentiles. In the figure, the variance can be seen to increase with decreasing SNR, until it is saturated due to the PRS maximum being weaker than the noise. For high SNR, the standard deviation is constant at about 0.02 due to side lobes in the PDP.

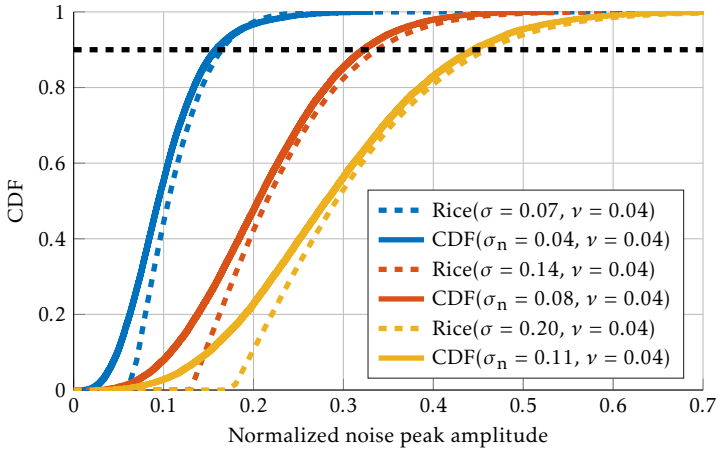

Figure 7.7: *Noise peak amplitude CDF and approximated truncated Rice CDF for peaks mostly unaffected by side lobes (the expected side lobe amplitude ν is low), for three different noise variance levels σ_n. The approximation can be seen to rarely underestimate the peak amplitude, which is paramount to suppress noise. A black dashed line indicates the level for the 90% threshold.*

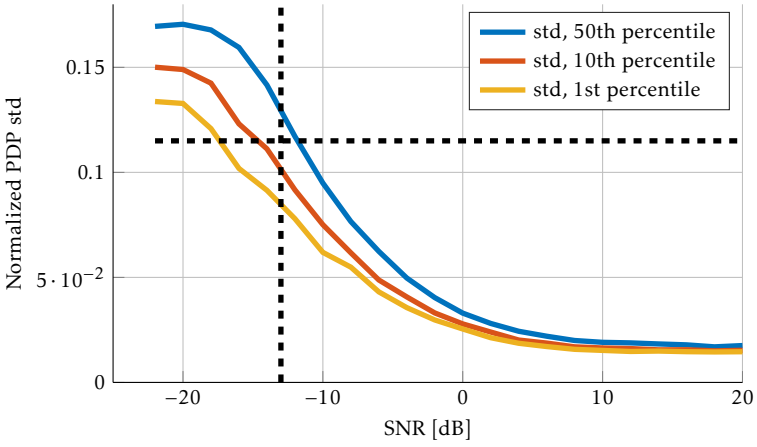

Figure 7.8: *PDP noise variance against SNR. Black dashed lines indicate the variance threshold used and conventional SNR threshold for hearability, 0.115 and −13dB respectively. The PDP noise variance can be seen to decrease as the SNR increases from noise dominated regions. For high SNR, the contribution of side lobes raises the noise PDP level from the expected levels. For low SNR, the variance stabilizes when the PDP maximum do not stem from the PRS.*

8

Discussion and Conclusion

In this chapter, the results and the method are discussed and the study questions presented in the problem formulation are answered.

8.1 Positioning Accuracy

The positioning accuracy acquired from the resulting TOA distributions showed significant improvements for a noise sensitive threshold when compared to a conventional constant threshold. When considering a single positioning occasion, allowing multiple uncertain TOA candidates increased the accuracy, mostly for the 90th percentile. When using the occasion with the highest likelihood value, the gain from multiple candidates was not as large.

The results proved that an appropriate detection threshold can drastically improve the accuracy of the TOA estimation, as well as the positioning. With multiple TOA candidates represented as a distribution, the probability of including a better candidate increased which in turn increased the positioning accuracy.

Combining of multiple measurement occasions were not tested, but the accuracy gain of lowered thresholds was indicated to be low when considering the performance of the best positioning occasion among eight. In the scenario with muting of PRSs, the positioning estimate with the highest likelihood value was similar for the cases of a single candidate and multiple candidates. This suggest that among the measurements, an early CIR peak was detected in at least one occasion. As this method of combining only considers the TOA candidates detected in one measurement occasion each, it can be seen as a pessimistic estimation of the case where the TOA distributions are combined across occasions. Also, it is probable that complete reports of eight occasions with positioning estimation is an inefficient approach. An alternative approach is proposed in the section for future work.

For the scenario without muting, the hearability of the PRS was very low, and too few BSs were detected to yield an accurate position for about 20% of the UEs. Although, for the detected BSs, the best TOA error was similar to the muted case. This vindicates the use of muting, as a large share of indoor UEs might become unable to be positioned otherwise.

8.2 Timing Accuracy

The timing accuracy, represented as the best TOA candidate error, was improved by introducing multiple TOA candidates. The accuracy gain was moderate for high SNR, and showed the largest TOA error reduction for low SNR. This is directly related to the threshold level, which determines the detectability of weaker CIR peaks. As the threshold was SNR sensitive, for high SNR there was little to be gained from a lower noise suppression. For low SNR, the CIR detectability improvement of a lower threshold was larger. Based on this, it might be sensible to lower the required noise suppression for higher noise levels, as the gains increases.

For high thresholds, above 90% noise peak suppression, the best TOA candidate reflected the positioning accuracy, as expected. This gives validity to the "best candidate" measurement when considering multiple candidates. The drawback of the best candidate measurement is that it does not consider the strength or noise probability of the candidates, which yields an overly optimistic metric for low noise suppression thresholds. Because of this, thresholds below 90% give too optimistic best TOA candidate performance. The best TOA candidate improves as the threshold is lowered. This is due to weak early multipath components being detected, and also partly due to noise peaks sometimes being a better choice. Although, if the candidate probability could be appropriately integrated into the best TOA metric, it would probably perform better also for low thresholds. However, the timing accuracy metrics are not essential to the actual positioning, so the gain of a better metric might not be significant.

8.3 Data Amount and Computational Complexity

The results suggested that the accuracy can be improved by using only a few extra peaks. The parameters of the method was only the PDP noise variance, and the peak amplitude and time delay. This study did not consider combined measurements, so to get the actual positioning accuracy of the best positioning occasion, multiple measurements for each BS would need to be sent. As many CIR peaks can be expected to be repeated among measurement occasions, a combining algorithm could compress this information to a large extent.

The computational complexity of the method was shown to depend exponentially on the number of BSs N used in the positioning. The exponential growth rate was determined by the number of TOA candidates K detected for each cell. For $K = 1$, the complexity is linear with N, but for higher K it rapidly increases. This highlights the trade-off between increased positioning accuracy on one hand,

and increased overhead and computation effort on the other. The complexity proved to be manageable, as only an average of 2.0 peaks were detected using the 90% threshold. Using a maximum of 14 BSs for the positioning, the computational complexity was on average less than 20000 times that of a single peak per BS.

Tests showed that the gain of additional detected BSs rapidly decreased after about 10 BSs. This suggests that additional BSs could be traded for additional TOA candidates. Optimization on accuracy versus complexity and on what peaks and BSs to keep could potentially be done at the Location Server.

To report the time estimates from UE to location server, a few formats come to mind as possibilities. Essentially, the reporting format could be amplitude based or probability based. The UE could report measured peak amplitudes along with time delays, or construct and report GMs for the time measurements. By keeping the amplitude of the peaks, the server side could potentially use more thorough probabilistic methods than the UE when constructing the GMs.

By allowing reports with a redundancy of BSs and TOA candidates, the computational effort and accuracy can be chosen arbitrarily at the server side. Another way to limit the complexity is to include a limit on the amount of reported BSs and TOA candidates. This would reduce the amount of redundant data transmitted, but require the UE to posses the logic to select the best set of measurements to include.

8.4 Parameter Selection

The proposed Probabilistic TOA Candidate Detection method was based mostly on modeling the PDP noise peak amplitude for inferring probability about each peak being a CIR path. Most method parameters could be verified against the measured noise distribution. However, the CIR probability assigned to a peak required assumptions beyond the noise distribution. The distance penalty factor α was the most uncertain parameter, as it were to represent the distribution of NLOS bias of the CIR peaks which should be assumed unknown if the radio environment of the UE is uncertain. If the parameter was left out, the positioning accuracy was degraded as distant noise peaks got too large weights, which in turn reduced the relative weight of the true CIR peaks. For LOS environments, the parameter should ideally be very large, but in NLOS conditions it should be limited to allow peaks before the strongest to be assigned non-zero weights. In this study, the parameter α yielded good results for values in the range from 2 to 5, but it is possible that the parameter is heavily dependent on environment.

8.5 Conclusions

Here, the questions posed in the problem formulation are answered.

Q How much does the positioning accuracy increase with several RSTD candidates?

A Using multiple RSTD candidates decreases the error to half for 90% of UEs when compared to a conventional method using a constant detection threshold of half the PDP maximum. Compared to a SNR sensitive threshold detecting a single first peak, the error is reduced by about a quarter for the percentiles 70% to 90%.

Q How much additional data need to be reported by the UE?

A Only an average of two TOA candidates were required in this study, which means the additional data are at most doubled, if no data apart from RSTD candidates are considered.

Q How much does the computational complexity increase at the UE and location server?

A Using 14 BSs for positioning, the computational complexity of using multiple candidates were less than 20 000 times that of a single candidate, which is still manageable.

8.6 Future Work

The results showed that the gain of lowering the detection threshold from 99.9% noise suppression to 90% was moderate, but significant. A test run for 50% threshold did not improve upon the 90% threshold; the suspected reason is that model assumptions were made for detection of peaks that were strong compared to noise, and applied heavy penalty to uncertain peaks when using low noise suppression.

In another variation, using the probability model for the peaks, the peak most probable of being the first path was used. For the 90% threshold, this yielded results similar to the 99.9% threshold using only the first peak, but with a local minor error increase between the 80% and 90% percentile. This reflects that the method can accurately assign a larger weight to certain CIR peaks, and smaller weights to peaks that are more uncertain.

An improvement on the proposed method would be to increase detectability for high SNR, as those measurements impacted the accuracy the most. As only the PDP was studied, side lobe contribution was hard to reduce and an increased threshold was applied. If the complex PRS cross correlation was considered in the method, more information would be available. Instead, each estimated delayed PRS copy received could be detected and subtracted from the cross correlation, allowing for a more effective side lobe removal. This detection and subtraction could be repeated until no peaks in a search window is above the detection threshold. This could potentially increase the detectability for high SNR significantly, for which the side lobe contribution is dominant. Also, peaks which appear close in time would more easily be distinguishable from each other after subtraction.

Apart from better side lobe suppression, the method could gain from subsample resolution in the time estimates. This should be considered in the cross correlation detection and subtraction to maximize the reduction of the subtracted

peak and its side lobes. However, it would invariably increase the accuracy with or without the additional cross correlation information.

This study only considered single occasions, but by combining several occasions, the accuracy should be expected to improve, to at least be about as accurate as the ML occasions. As the probability of each detected peak being noise has been estimated in the study, it should be straightforward to combine multiple positioning occasions. For example, the probability of each time delay being noise could be modeled as an inverse GM, where the base probability is one and the amplitude of peaks reduce the noise probability. The probability of each time delay being noise could then be directly obtained as the probability product. Finally, in the resulting probability function, candidates could be selected by a threshold detection similar to the one used in this study.

A final remark is made on the possibilities of alternative distributions for the time estimates. In this study, the TOA candidates were represented as a GM, and the candidate weight were applied an exponential penalty based on distance to a confident CIR peak. Although, as the NLOS bias always is positive, a Gaussian distribution for the TOA candidates might be suboptimal. Instead, an exponential mixture or similar could potentially improve the accuracy by reflecting the higher probability of detecting a TOA candidate after the LOS than before.

Bibliography

[1] *An Overview of LTE Positioning*. Spirent, Feb. 2012.

[2] Pi-Chun Chen. "A non-line-of-sight error mitigation algorithm in location estimation". In: *1999 IEEE Wireless Communications and Networking Conference, 1999. WCNC* (1999), 316–320 vol.1.

[3] L. Cong and W. Zhuang. "Nonline-of-sight error mitigation in mobile location". In: *INFOCOM 2004. Twenty-third AnnualJoint Conference of the IEEE Computer and Communications Societies* 1 (Mar. 2004), p. 659.

[4] Li Cong and Weihua Zhuang. "Non-line-of-sight error mitigation in TDOA mobile location". In: *IEEE Global Telecommunications Conference, 2001. GLOBECOM '01* 1 (2001), 680–684 vol.1.

[5] *Coordinated multi-point operation for LTE physical layer aspects, Release 11*. TR 36.819. 3GPP.

[6] J.A. Del Peral-Rosado et al. "Achievable localization accuracy of the positioning reference signal of 3GPP LTE". In: *2012 International Conference on Localization and GNSS (ICL-GNSS)* (June 2012), pp. 1–6.

[7] Sven Fischer. *Observed Time Difference Of Arrival (OTDOA) Positioning in 3GPP LTE*. Qualcomm Technologies, Inc, June 6, 2014.

[8] *Further advancements for E-UTRA phyical layer aspects*. Technical Report 36.814. 3GPP, Mar. 2010, pp. 90–102.

[9] N. El Gemayel, S. Meier, and F. K. Jondral. "On the applicability of the residual weighting algorithm for TDOA". In: *2012 4th International Congress on Ultra Modern Telecommunications and Control Systems and Workshops (ICUMT)* (Oct. 2012), pp. 143–147.

[10] F. Gustafsson and F. Gunnarsson. "Mobile positioning using wireless networks: possibilities and fundamental limitations based on available wireless network measurements". In: *IEEE Signal Processing Magazine* 22.4 (July 2005), pp. 41–53.

[11] Ming Huang and Wen Xu. "Enhanced LTE TOA/OTDOA estimation with first arriving path detection". In: *2013 IEEE Wireless Communications and Networking Conference (WCNC)* (Apr. 2013), pp. 3992–3997.

[12] *Initial calibration results for 3D channel model*. R1-135767. Ericsson, Nov. 2013.

[13] S. Al-Jazzar, J. Caffery, and H. R. You. "Scattering-Model-Based Methods for TOA Location in NLOS Environments". In: *IEEE Transactions on Vehicular Technology* 56.2 (Mar. 2007), pp. 583–593.

[14] S. Al-Jazzar, J. Caffery, and H.-R. You. "A scattering model based approach to NLOS mitigation in TOA location systems". In: *Vehicular Technology Conference, 2002. VTC Spring 2002. IEEE 55th* 2 (2002), 861–865 vol.2.

[15] Regina Kaune. *Gaussian Mixture (GM) Passive Localization using Time Difference of Arrival (TDOA)*. 2009.

[16] C. Knapp and G.Clifford Carter. "The generalized correlation method for estimation of time delay". In: *IEEE Transactions on Acoustics, Speech and Signal Processing* 24.4 (Aug. 1976), pp. 320–327.

[17] J. Li, J. Conan, and S. Pierre. "Mobile Terminal Location for MIMO Communication Systems". In: *IEEE Transactions on Antennas and Propagation* 55.8 (Aug. 2007), pp. 2417–2420.

[18] D. Liu et al. "Analysis of Wireless Localization in Nonline-of-Sight Conditions". In: *IEEE Transactions on Vehicular Technology* 62.4 (May 2013), pp. 1484–1492.

[19] F. Muhammad and H. Li. "Localization of mobile transmitting devices in non Line-of-Sight (NLOS) multipath environments using MIMO radar technology". In: *2014 IEEE Symposium on Wireless Technology and Applications (ISWTA)* (Sept. 2014), pp. 24–29.

[20] Y. Oualil et al. "A TDOA Gaussian mixture model for improving acoustic source tracking". In: *Signal Processing Conference (EUSIPCO), 2012 Proceedings of the 20th European* (Aug. 2012), pp. 1339–1343.

[21] K. Pahlavan, Xinrong Li, and J.-P. Makela. "Indoor geolocation science and technology". In: *IEEE Communications Magazine* 40.2 (Feb. 2002), pp. 112–118.

[22] R. Rahdar, J. T. Stracener, and E. V. Olinick. "A Systems Engineering Approach to Improving the Accuracy of Mobile Station Location Estimation". In: *IEEE Systems Journal* 8.1 (Mar. 2014), pp. 14–22.

[23] H. Ryden et al. "Baseline performance of LTE positioning in 3GPP 3D MIMO indoor user scenarios". In: *2015 International Conference on Localization and GNSS (ICL-GNSS)* (June 2015), pp. 1–6.

[24] C. K. Seow and S. Y. Tan. "Non-Line-of-Sight Localization in Multipath Environments". In: *IEEE Transactions on Mobile Computing* 7.5 (May 2008), pp. 647–660.

[25] *Study on 3D channel model for LTE, Release 12*. TR 36.873. 3GPP.

[26] *Study on indoor positioning enhancements for UTRA and LTE*. TR37.857. 3GPP, Feb. 2015.